Bull Volcanol (2001) 63:20–44
DOI 10.1007/s004450000120

RESEARCH ARTICLE

Andrew J. L. Harris · S. K. Rowland

FLOWGO: a kinematic thermo-rheological model for lava flowing in a channel

Received: 31 July 2000 / Accepted: 6 November 2000 / Published online: 17 February 2001

Abstract We present a kinematic, self-adaptive, numerical model to describe the down-flow thermal and rheological evolution of channel-contained lava. As our control volume of lava advances down a channel it cools and crystallizes, an increasingly thick and extensive surface crust grows, and its heat budget and rheology evolve. By estimating down-flow heat and velocity loss, our model calculates the point at which the control volume becomes stationary, giving the maximum distance lava flowing in the channel can extend. Modeled effusion rates, velocities, widths, surface crust parameters, heat budget, cooling, temperature, crystallinity, viscosity, and yield strength all compare well with field data collected during eruptions at Mauna Loa, Kīlauea, and Etna. Modeled lengths of 25–27, 2.5–5.7, and 0.59–0.83 km compare with measured lengths of 25–27, 4, and 0.75 km for the three flows, respectively. Over proximal flow portions we calculate cooling, crystallization, viscosity, and yield strength of 1–10 °C km^{-1}, 0.001–0.01 volume fraction km^{-1}, 10^3–10^4 Pa s, and 10^{-3}–10^2 Pa, respectively. At the flow front, cooling, crystallization, viscosity, and yield strength increase to >100 °C km^{-1}, 0.1 volume fraction km^{-1}, 10^6–10^7 Pa s, and 10^3–10^4 Pa, respectively, all of which combine to cause the lava to stop flowing. Our model presents a means of (a) analyzing lava flow thermo-rheological relationships; (b) identifying important factors in determining how far a channel-fed flow can extend; (c) assessing lava flow hazard; and (d) reconstructing flow regimes at prehistoric, unobserved, or remote flows.

Keywords Lava flow · Cooling · Crystallization · Rheology · Mauna Loa · Kīlauea · Etna

Editorial responsibility: T.H. Druitt

A. J. L. Harris (✉) · S. K. Rowland
HIGP/SOEST, University of Hawai'i, 2525 Correa Road, Honolulu, Hawai'i 96822, USA
E-mail: harris@pgd.hawaii.edu
Phone: +808-9563157
Fax: +808-9566322

Introduction

How far can channelized or leveed lava flow? The answer to this question is crucial if we are to fully understand the thermal and rheological characteristics of channelized lava. This understanding is also imperative when assessing the hazard posed by an active channelized flow. It is well known that channelized lava flows can extend many kilometers in a relatively short time. For example, during the 1984 eruption of Mauna Loa (Hawai'i) lava erupting at volumetric effusion rates of 800 to 140 m^3 s^{-1} fed channelized flows which extended 25 km in 5 days, reaching to within 6 km of the outskirts of Hilo (Lipman and Banks 1987; Lockwood et al. 1987). Determining the eruptive and flow characteristics required for the flow to have reached Hilo proper would be useful for volcanic risk assessment. The reverse question is posed by consideration of lava flows that were not observed while they were active: Can the thermal, rheological, and environmental characteristics of these flows be modeled based on knowledge of available flow parameters such as underlying slopes and channel dimensions?

Numerous previous models have been constructed dealing with various aspects of flow emplacement and cooling. These show, for example, how flow length, volumetric flow rate, and velocity are influenced by channel dimensions, lava cooling, crystallization, and related rheological parameters (Dragoni et al. 1986; Dragoni 1989; Dragoni et al. 1992; Dragoni and Tallarico 1994; Pinkerton and Wilson 1994; Keszthelyi 1995a; Tallarico and Dragoni 1999). Other previous models have linked temperature, crystallinity, and rhe-

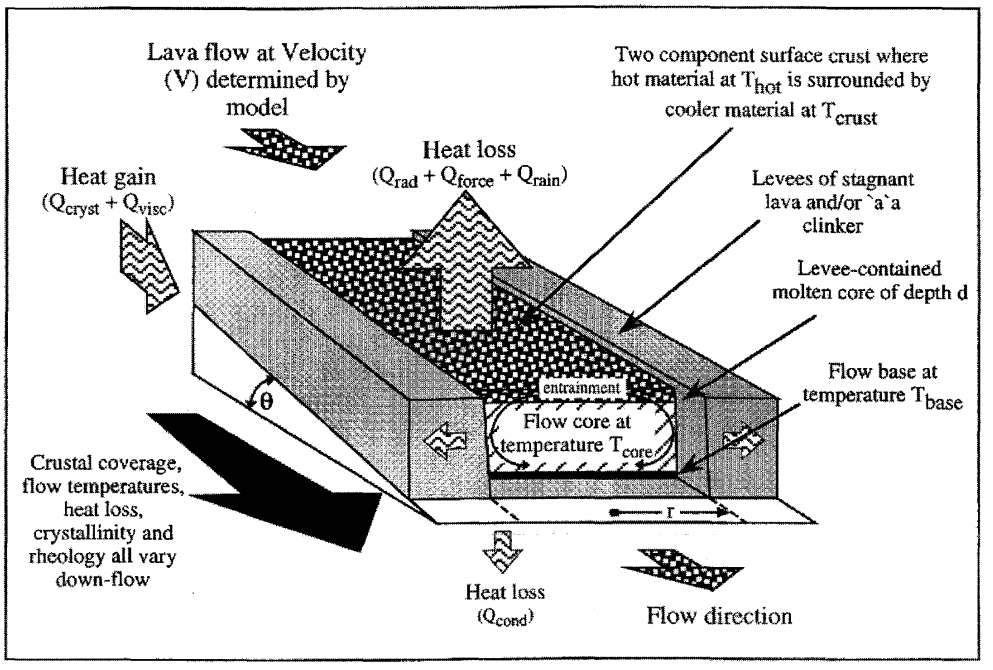

Fig. 1 Summary of the thermo-rheological model (FLOWGO). The control volume of channel-contained lava is advanced and cooled in 1-m increments. With each cooling step the interrelated thermal, crystal, and rheological characteristics of the control volume are recalculated until the velocity drops to zero or the core temperature reaches solidus. Crystallinity, temperature, and rheology are determined by the heat balance, where the various heat gains and losses during flow allow us to determine changes in lava temperature and crystallinity, and hence rheology. An increasingly thick and extensive crust is grown down-flow as velocity decreases and the channel increases in width as it slows to conserve volume

ology (Pinkerton and Sparks 1978; Dragoni et al. 1986; Pinkerton and Stevenson 1992; Dragoni and Tallarico 1994). Keszthelyi (1995a), Keszthelyi and Denlinger (1996), and Klingelhöfer et al. (1999) have constructed thermal models for flow in tubes, at pāhoehoe lobes, and in submarine lava tubes (pillows), respectively. Dragoni (1989), Crisp and Baloga (1990), Ishihara et al. (1990), Harris et al. (1998), Keszthelyi and Self (1998), and Cashman et al. (1999) have produced heat loss models for channelized and 'a'ā lava flows.

Most of these previous models either consider only heat loss by radiation, ignore the contribution of heat losses from the crusted surface component, or do not link heat loss to lava cooling, crystallization, and subsequent rheological changes. Here our aim is to take into account all of these factors and to link the many thermal and rheological models to produce an integrated thermo-rheological model for lava flowing in a channel (Fig. 1). In doing this we seek to (a) describe and analyze the inter-relationships between underlying topography, channel dimensions, crustal formation, flow thermal regime, crystallinity, lava rheology, and velocity; and (b) determine how each parameter varies down-flow. This in turn will allow an approximation of how far channelized lava can flow and what effusion rates are required to feed the flow. We test the model against three well-documented cases: The 1984 flow of Mauna Loa (Hawai'i); a May 1997 flow from Pu'u 'Ō'ō (Kilauea, Hawai'i); and an October 1998 flow from Etna's SE crater (Sicily).

Because forward motion of the flow is critically dependent upon these rheological parameters, they will determine whether a flow can move and consequently how far it can extend. A well-insulated flow will have a lower rate of heat loss and crystallization than a poorly insulated flow, so its viscosity and yield stress will increase less rapidly. For a given effusion rate over a constant slope, a well-insulated flow will extend farther than a poorly insulated flow. Flow insulation is determined by the extent and temperature of any surface crust that develops. An entirely roofed (i.e., tubed) flow will give lowest rate of heat loss and allow a flow to extend much greater distances than in open channels (Dragoni et al. 1995; Keszthelyi 1995a; Keszthelyi and Self 1998). The amount of crust (or whether or not a continuous crust can develop at all), however, is controlled largely by velocity-related tearing, disruption, and foundering. There is obviously a complex interplay between the processes that occur during lava flow emplacement and it is the challenge of the modeler to describe and link all such processes.

Model principles

The velocity of lava flowing in a channel depends on the rheological properties of the lava (density, viscosity, yield strength), environmental factors (gravity, underlying slope), and the channel dimensions. Lava viscosity and yield strength can, in turn, be related to lava temperature and crystallinity (Pinkerton and Sparks 1978; Dragoni et al. 1986; Pinkerton and Stevenson 1992; Dragoni and Tallarico 1994). Thus, in our model, FLOWGO, as a control volume advances down the channel it cools and crystallizes, causing its temperature- and crystallinity-dependent rheological factors to change (Fig. 1). We continue to advance the control volume down the channel until either velocity drops to zero or the lava core temperature reaches the solidus. To model the complex interplay between the

many thermo-rheological processes that occur during lava flow, we make four initial simplifying assumptions.

Channelized flow

Our modeled flow is channelized, meaning the fluid, moving lava is contained between stagnant levees and has no mechanically continuous roof. The top of the moving lava therefore represents a free surface open to the atmosphere, but its sides and bottom are in contact with levee walls and the emplaced flow base. In the case of lava flowing in a mature and stable channel, the banks and base will be stagnant and mechanically stable. Farther downslope the fluid, molten core will be flowing between levees of 'a'ā clinker that may or may not be stationary (e.g., Sparks et al. 1976; Lipman and Banks 1987). Our model is able to accommodate these channel morphology differences whereby a proximal channel of fluid lava with distinct stagnant levees evolves down-flow into a shear-zone-contained 'a'ā flow (e.g., Figs. 2, 3).

Conservation of mass by channel widening

Our control volume does not lose mass. It advances down-channel in 1-m increments and changes its velocity as viscosity and yield strength increase and as the underlying slope changes. The starting effusion rate is given by at-vent channel width and depth (input from field accounts) and a calculated starting velocity based on these dimensions. From then on we hold depth (d) constant and conserve mass (m) by varying channel width (w) as velocity (V) changes:

$$m = \rho_{lava} dwV = \text{constant}, \quad (1)$$

in which ρ_{lava} is lava density. Thus, if the control volume slows, the channel widens. Because velocity is also related to slope, this results in a channel that becomes slower and wider when the underlying slope is gradual. This was a characteristic of both the 1984 Mauna Loa and 1998 Etna flows. Additionally, Gregg and Fink (2000) have shown a clear inverse relationship between underlying slope and flow width.

Channel-contained control volume

For simplicity, we model a single control volume flowing in a channel that lags (by an unspecified distance) behind, and is unimpeded by, the flow front. The model allows the control volume to fully evolve thermally and structurally down channel. Thus, although the initial starting channel conditions are unlike those at the flow front, by the end of each model run the control volume essentially becomes the flow front. Our model terminates when velocity becomes zero. The control volume has reached its maximum, cooling-limited extent. Among our FLOWGO results are the starting channel dimensions required to carry the control volume a particular distance given our modeled thermal and rheological constraints.

Three-component vertical thermal structure

Our model lava element consists of three thermal zones from top to bottom: surface, core, and base (Fig. 1). The surface consists of a chilled crust which, following Crisp and Baloga (1990), is broken by areas where higher temperature material is exposed. FLOWGO allows crust coverage and temperature to evolve down-flow. The crust cools while at the same time increasing in areal coverage and thickness. The core is the isothermal high temperature interior that also cools down-flow. The base consists of a cooler, basal crust. Heat is lost from the core control volume through the surface and basal crust layers.

Case comparisons

We selected three examples to illustrate the morphologies that we are modeling and against which we test the validity of our model: the 1984 Mauna Loa flow (Hawai'i); the 16 May 1997 Pu'u 'Ō'ō' flow; (Kīlauea, Hawai'i) and the 11–12 October 1998 Mt. Etna flow (Italy). These were all channel-fed 'a'ā flows and include a range of lengths and underlying slopes (allowing a thorough test of our model). Importantly, many rheological, thermal, and dimensional measurements were made on these flows and can be used to validate our results.

Case 1: Mauna Loa 1984

The 25 March to 14 April 1984 northeast rift eruption of Mauna Loa emplaced a 25- to-27-km-long channel-fed basaltic 'a'ā flow system over underlying slopes ranging between 1 and 9°. The following narrative for this eruption is taken from Lockwood et al. (1985) and Lipman and Banks (1987). After an initial phase of activity within the summit caldera and at the 3500-m elevation, an eruptive fissure opened between 2770 and 2930 m on 25 March. Four flows advanced down slope to the east, with the three southerly flows stagnating by 27 March. The most northerly flow (flow 1), however, continued to advance, reaching the 915-m level, 25 km from the vent, by 29 March (Fig. 2). During the morning of 29 March a blockage at the 1800-m level robbed flow 1 of its supply and fed a new flow (flow 1A) which eventually stagnated 27 km from its source (Fig. 2). Lava production began to decline on 7 April causing the distal portion of the system to stag-

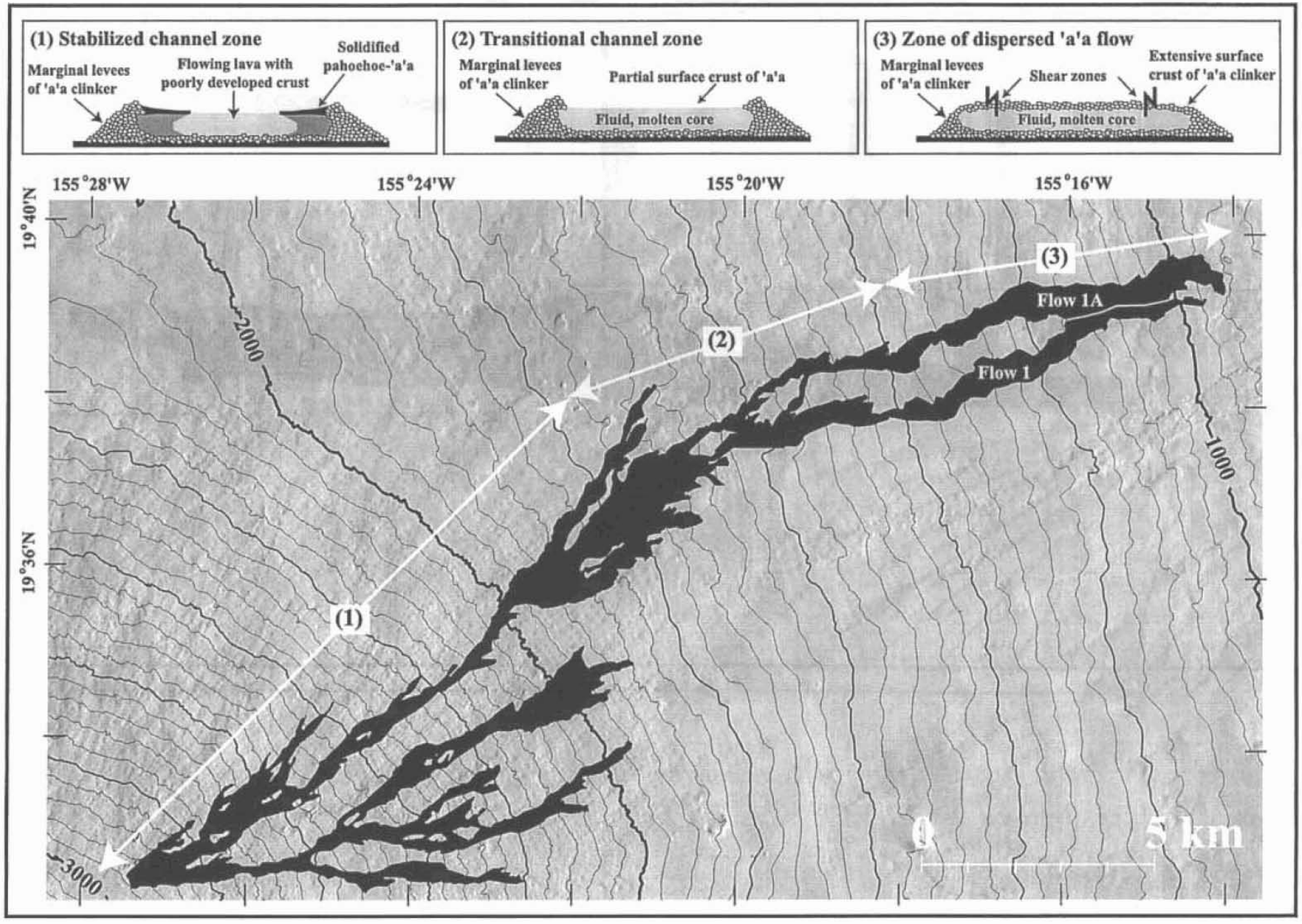

Fig. 2 Flow map of the Mauna Loa 1984 flow adapted from Wolfe and Morris (1996) and projected onto a shaded relief map (contour interval 40 m). The locations of three main morphological zones defined for this flow are indicated and summarized at the top

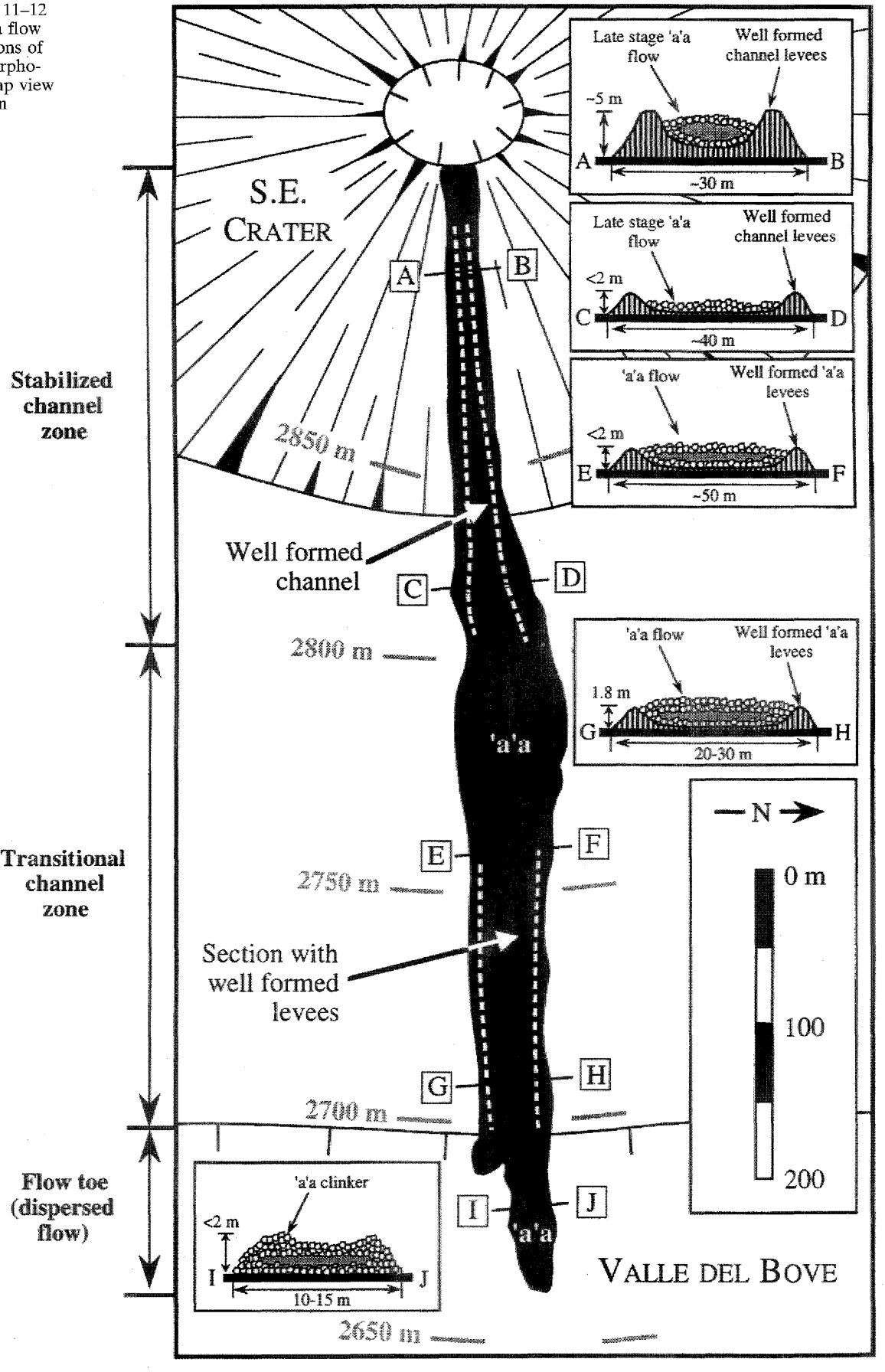

Fig. 3 Map of the 11–12 October 1998 Etna flow showing the locations of the three main morphological zones in map view and in cross section

nate, with activity confined to within 2 km of the vent by 13 April, and ceasing all together on 14 April.

During this eruption extensive measurements were made of channel dimensions, channel and flow-front velocity, yield strength, viscosity, vesicularity, density, temperature, and crystallinity. These data are given by Lipman and Banks (1987), Moore (1987), and Crisp et al. (1994). Based on systematic down-flow variations in the structure and morphology of the 'a'ā flows, Lipman and Banks (1987) defined four zones for this channel-fed 'a'ā flow system: flow toe; lower dispersed flowage; transitional channel; and upper stabilized channel. This system forms the basis of our flow model and is illustrated in Fig. 2, where we combine the flow toe and zone of dispersed flow into one zone.

Stabilized channel (proximal) zone

Within the upper reaches of the flow all movement became concentrated in a central channel of stable geometry. By 28–29 March this zone extended ~10 km from the vent and comprised ~40% of the flow length.

Transitional channel (medial) zone

Transitional channel zone was marked by a distinct channel containing incandescent clinkery 'a'ā lava. Here and in the stabilized channel zone, flow was bounded by levees of 'a'ā clinker. These levees were modified later by channel overflows, accretion, and deformation. By 28 March this zone extended upflow 5–10 km from approximately 1–2 km behind the flow front and comprised 20–40% of the flow system.

Zone of dispersed flow and flow toe (distal zone)

The flow toe consisted of a broad flow front of'a'ālava. Behind this movement was dispersed across much of the flow width and a distinct channel rarely developed, although shear zones indicated localized velocity discontinuities. On 27 March this zone extended ~1 km up flow from the toe, but as the eruption progressed it extended 5–10 km upflow and comprised 20–40% of the flow system.

Case 2: Pu'u 'Ō'ō 16 May 1997

The 16 May 1997 flow at Pu'u 'Ō'ō is described by Cashman et al. (1999). It was fed from a vent on the flank of the Pu'u 'Ō'ō cone and extended 4 km over 2–10° slopes. The channel was typically <3 m deep and 5–10 m wide with 50-m-wide complex levees built of 'a'ā and pāhoehoe spillovers. The lava flowing in the channel had a smooth surface from the vent out to 1.7–1.9 km, and beyond this the surface consisted of clinkers and broken solid plates. Downflow temperature and crystallinity are presented by Cashman et al. (1999).

Case 3: Mt. Etna, 11–12 October 1998

During the night of 11–12 October 1998 an episode of intense strombolian activity at Mt. Etna's SE crater fed basaltic–andesite lava down the 18–30° eastern flank of the cone (GVN 1999a). Mapping on 14 October showed that this event emplaced a single 755-m-long 'a'ā flow that could be divided into a similar three zone morphological system to that of the 1984 Mauna Loa flow (Fig. 3).

The proximal portion of the flow consisted of a distinct channel bounded by 5-m-high banks of 'a'ā clinker and containing a late-stage 5- to 15-m-wide 'a'ā flow that had not drained out from the channel (Fig. 3). The distinct channel zone extended 320 m to just beyond the base of the SE crater (where a distinct decrease in slope occurs) and comprised 42% of the flow length. The medial portion consisted of a transitional channel zone. Here the channel banks were lower than in the distinct channel zone and, in places, poorly defined (Fig. 3). The transitional zone extended 325 m to the break in slope that marks the back wall of the Valle del Bove (where the underlying slope increases sharply), and accounted for 43% of the flow length. The final 110 m (15%) of the flow, the distal zone, was an 'a'ā flow up to 2 m thick at its margins but slightly thinner at the center (Fig. 3).

The FLOWGO model

In the following sections we discuss the different aspects of the FLOWGO model including how each parameter is calculated and how it relates to other parameters. Once these parameters are defined, FLOWGO evolves the control volume and tracks the temperature and cooling of the core until it reaches solidus or becomes too viscous to advance.

Velocity in terms of viscosity and yield strength (V, η, YS):

Following Moore (1987), mean velocity (V) is calculated for a Bingham fluid flowing in a semicircular channel from

$$V = (r^2 \rho_{lava} g \sin\theta / 8\eta)[1-(4/3)(YS_{core}/YS_{base}) + (1/3)(YS_{core}/YS_{base})^4] \quad (2a)$$

or in channel which is much wider than it is deep from

$$V = (d^2 \rho_{lava} g \sin\theta / 3\eta)[1-(3/2)(YS_{core}/YS_{base}) + (1/2)(YS_{core}/YS_{base})^3] \quad (2b)$$

Table 1 Constants used in the FLOWGO model. All values given are those used by us for the Mauna Loa case. Values change depending on lava composition and volcano

Term	Definition	Value or source
a	Constant given by Dragoni (1989)	0.04 K^{-1}
α_{air}	Thermal conductivity of air	Kays and Crawford (1980)
α_{lava}	Thermal conductivity of basalt[c]	Calculated following Peck (1978, p 41; W m^{-1} K^{-1})
b	Constant given by Dragoni (1989)	10^{-2} Pa
β_{air}	Thermal diffusivity of air	Kays and Crawford (1980)
c	Constant given by Dragoni (1989)	0.08 K^{-1}
C_H	$=(U^*/U)^2$ where U^* is friction wind speed[a]	0.0036[b]
cp_{air}	Specific heat capacity of air	1099 J kg^{-1} K^{-1}
cp_{lava}	Specific heat capacity of basalt[c]	1225 J kg^{-1} K^{-1}
ε	Emissivity of basalt	0.95
g	Acceleration due to gravity	9.8 m s^{-2}
η_{air}	Viscosity of air	Kays and Crawford (1980)
η_{erupt}	Lava viscosity at eruption temperature	1000 Pa s[d]
κ_{air}	Cubic expansivity of air	Kays and Crawford (1980)
L_{cryst}	Latent heat of crystallization	$3.5\pm0.7\times10^5$ J kg^{-1}
L_{H2O}	Latent heat of vaporization plus heat needed to raise water temperature to 100°C	2.8×10^6 J kg^{-1}
ρ_{air}	Density of air	0.4412 kg m^{-3}
ρ_{H2O}	Density of water at 100°C	958 kg m^{-3}
ρ_{lava}	Density of basalt[c]	2600 kg m^{-3}
σ	Stefan-Boltzmann constant	5.67×10^{-8} W m^{-2} K^{-4}

[a]From Keszthelyi and Denlinger (1996)
[b]From Greeley and Iverson (1987)
[c]Value given is for dense rock, all values used by us were corrected for vesicularity (see Tables 2, 5) or were calculated as a function of vesicularity using the relationship given in Peck (1978), $cp_{lava}=(1.929–1.554\ Ves)^2$
[d]At-vent viscosity for basalt with a liquidus ~1200°C and T_{erupt} ~1140°C calculated from Dragoni (1989)

in which r and d are the channel radius and depth, g is acceleration due to gravity, θ is slope, ρ_{lava} and η are lava density and viscosity, and YS_{core} and YS_{base} are the yield strengths of the core and base, respectively (Tables 1, 2). We use Eq. (2a) when $r \leq d$ and Eq. (2b) when $r>d$. We assume that the lava density is insensitive to temperature so that the only temperature-dependent terms in Eq. (2a, 2b) are viscosity and yield strength. Motion will cease when V=0.

Viscosity and yield strength in terms of temperature and crystallinity (η, YS, ϕ_{total})

Crystallinity changes are important for two reasons. First are the rheological effects of microlites on viscosity and yield strength. Secondly, the latent heat of crystallization is an important heat-gain term for the control volume. Following the relationships given by Pinkerton and Stevenson (1992) and Dragoni (1989), bulk viscosity of the flowing core (η) can be calculated as a function of temperature and crystal content from

$$\eta = \{[1-R\phi_{total}]^{-2.5}\}\{\eta_{erupt}\exp[a(T_{erupt}-T_{core})]\} \quad (3)$$

in which T_{core} and ϕ_{total} are core temperature and mass fraction of crystals, R is the inverse of the maximum crystal concentration that will still allow flow (Pinkerton and Stevenson 1992), η_{erupt} is the viscosity of lava at eruption temperature T_{erupt}, and a is a constant (Tables 1, 2).

Following Pinkerton and Stevenson (1992) and Dragoni (1989), bulk yield strength (YS) can be calculated as a function of temperature and crystal content from

$$YS_{core} = \{6500\phi_{total}^{2.85}\} + b\{\exp[c(T_{erupt}-T_{core})-1]\} \quad (4a)$$

and

$$YS_{base} = \{6500\phi_{base}^{2.85}\} + b\{\exp[c(T_{erupt}-T_{base})-1]\}, \quad (4b)$$

in which YS_{core} and YS_{base} are the yield strengths in the core and base of the flowing portion of lava, respectively, b and c are constants, and ϕ_{base} is the mass fraction of microlites in the basal crust (Tables 1, 2).

Down-flow variation in microlite crystallinity (ϕ_{micro})

We assume a linear inverse relationship between microlite crystallinity and temperature once the lava leaves the vent:

$$\delta\phi_{micro}/\delta x = (\delta T/\delta x)(\delta\phi_{micro}/\delta T) \quad (5a)$$

where $\delta\phi_{micro}/\delta x$ and $\delta T/\delta x$ are microlite increase per unit length and core temperature decrease per unit length, respectively. $\delta\phi_{micro}/\delta T$ is the increase in microlites per degree of cooling, and is determined by assuming that the difference in microlite abundance (ϕ_{post}) between an at-vent sample and a distal sample was the result of cooling across the temperature interval from T_{erupt} to T_{solid} ($=T_{cool}$):

Table 2 Variables used in FLOWGO. Given are values used for the Mauna Loa 1984 flow. Values change depending on eruption case, lava composition, and volcano. (Changes to these values to take into account the differing cases at Kīlauea and Etna are given in Table 5.)

Term	Definition	Value	Source
A	Planimetric area of control volume	Variable down-flow	=w L
D	Channel depth	5.5±0.5 m	Lipman and Banks (1987)
ΔT_{base}	Core – base temperature difference	Variable down-flow	$=T_{core}-T_{base}$
ΔT_{surf}	Temperature difference between the lava surface and ambient air	Variable down-flow	$=[f_{crust}T_{crust}^{1.3}+f_{hot}T_{hot}^{1.3}]^{0.75}-T_{air}$
$\delta R/\delta t$	Rainfall rate	7.93×10^{-8} m s^{-1}	Keszthelyi (1995a)
$\delta T/\delta x$	Temperature change per unit length	Variable down-flow (K m^{-1})	Eq. (7a, 7b)
$\delta\phi_{micro}/\delta x$	Fraction of crystallization per unit length	Variable down-flow	Eq. (5a, 5b)
E	Entrainment rate	Variable down-flow (m^3 s^{-1})	Appendix
E_r	Effusion rate	Constant down-flow (m^3 s^{-1})	=w d V
f_{crust}	Surface fraction occupied by crust	Variable down-flow	Eq. (8)
f_e	Fraction of E_r which is entrained	0.01–0.25	Crisp and Baloga (1994)
f_{hot}	Surface fraction occupied by exposed core	Variable down-flow	$=1-f_{crust}$
η	Lava viscosity	Variable down-flow (Pa s)	Eq. (3)
H_b	Thickness of basal crust	10±9% of flow depth	Field observations
H_c	Thickness of core	Variable down-flow (m)	$=d-H_b-H_s$
H_s	Thickness of surface crust	Variable down-flow (m)	Appendix
L	Control volume length	1.0 m	
θ	Slope	0–10 km=5–7°, then 3–4°	DEM (Fig. 5a)
R	Inverse of maximum solids concentration	1.51±0.16	From data in Pinkerton and Stevenson (1992)
r	Channel radius	1.85±0.45 m	Lipman and Banks (1987)
T_{air}	Ambient air temperature	293 K (20±10°C)	Typical for Hawai'i
T_{base}	Temperature at base of basal crust	973±200 K (700±200°C)	Keszthelyi (1995b); Wooster et al. (1997)
T_{cool}	Down-flow cooling	160±13 K[a]	$=T_{crupt}-T_{solid}$
T_{core}	Flow core temperature	Variable down-flow (K)	
T_{crust}	Temperature of crust	Variable down-flow (K)	
T_e	Effective radiation temperature	Variable down-flow	$=(f_{crust}T_{crust}^{4}+f_{hot}T_{hot}^{4})^{0.25}$
T_{erupt}	Eruption temperature	1413 K (1140±3°C)	Lipman and Banks (1987)
T_{hot}	Temperature of exposed molten lava	Variable down-flow (K)	Eq. (9)
T_{solid}	Solidus temperature	1253 K (980±10°C)	Peck (1978)
τ	Surface crust survival time	Variable down-flow (s)	Appendix
τ_e	Time for total exchange of core and crust	Variable down-flow (s)	Appendix
U	Wind speed	5.0 m s^{-1}	Typical for Hawai'i
V	Flow velocity	Variable down-flow (m s^{-1})	Eq. (2a, 2b)
Ves	Volume fraction of vesicles	0.08±0.07	Lipman and Banks (1987)
w	Channel width	31±26 m	Lipman and Banks (1987)
YS_{core}	Yield strength of lava core	Variable down-flow (Pa)[e]	Eq. (4a)
YS_{base}	Yield strength of lava base	Variable down-flow (Pa)[e]	Eq. (4b)
ϕ_{base}	Mass fraction of solids in basal crust	1.0	Assumes crust is solid
ϕ_{phen}	Mass fraction of crystals upon eruption	0.15±0.15	Lipman and Banks (1987)
ϕ_{post}	Total microlites grown between vent and distal end of flow	0.45±0.25	From Lipman and Banks (1987), Crisp and Baloga (1994), Crisp et al. (1994)
ϕ_{micro}	Mass fraction of microlites grown since eruption	Increases down-flow	Eq. (6a)
ϕ_{total}	Mass fraction of pre-eruption and grown crystals at distance × down-flow	Increases down-flow	Eq. (6b)

[a]In agreement with Archambault and Tanguy (1976) who give 150–200 °C as the liquidus–solidus difference for most magmas

$$\delta\phi_{micro}/\delta T = \phi_{post}/T_{cool}. \quad (5b)$$

We can now calculate the mass fraction of microlites grown between the vent and any down-flow distance x from

$$\phi_{micro}(x) = \int_0^x (\delta\phi_{micro}/\delta x)\delta x\,. \quad (6a)$$

To obtain the total crystal content at any point along the flow, the mass fraction of phenocrysts and microphenocrysts grown prior to eruption (ϕ_{phen}) must be added to Eq. (6a) so that:

$$\phi_{total}(x) = \phi_{phen+}\phi_{micro}(x)\,. \quad (6b)$$

Down-flow variation in temperature (ΔH, Q)

Down-flow lava temperature variation ($\delta T/\delta x$) is determined by the interplay between processes that remove heat from within the control volume and those which add heat to it. Heat is lost from the control volume top by radiation (Q_{rad}), rain falling on the lava surface (Q_{rain}), and forced or free convection (Q_{force} or Q_{free}) where, following Head and Wilson (1986), we

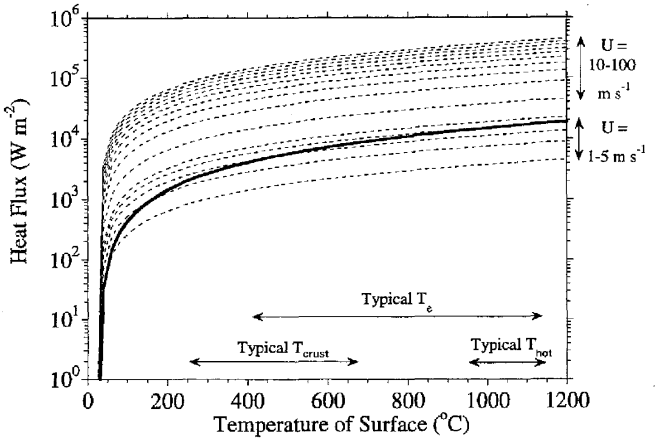

Fig. 4 Relationship between heat loss to convection and surface temperature. Free convection heat loss is given by the *thick solid line*. Forced convection (*dashed lines*) is given for a range of wind velocity (U). Note that forced convection dominates at velocities greater than ~5 m s^{-1}

use whichever is greater (Fig. 4). Heat is also lost by conduction through the basal crust (Q_{cond}). Heat is supplied by latent heat of crystallization (Q_{cryst}) and viscous dissipation (Q_{visc}). Each of these terms can be described and calculated using standard heat transfer physics previously applied to lava flows by, for example, Danes (1972), Head and Wilson (1986), Dragoni (1989), Crisp and Baloga (1990), Oppenheimer (1991), Crisp and Baloga (1994), Keszthelyi (1995a), Keszthelyi and Denlinger (1996), Harris et al. (1997, 1998), and Keszthelyi and Self (1998). These terms, as rewritten and used by us, are given in Table 3.

All the heat lost from the control volume passes through the basal and top surfaces to the environment. This heat loss is partially balanced by heat produced within the control volume so that the change in heat content of a unit length per unit time (ΔH) is described by

$$\Delta H = -Q_{cond}-Q_{rad}-Q_{force}-Q_{rain+}Q_{cryst+}Q_{visc}. \quad (7a)$$

By using Eq. (7a) with the relationships given in Table 3 (and re-arranging the Q_{cryst} term to isolate $\delta T/\delta x$), down-channel cooling per unit length ($\delta T/\delta x$) can be calculated from:

$$\delta T/\delta x = [-Q_{rad}-Q_{force}-Q_{rain+}Q_{visc}]/[\ E_r\rho_{lava}L_{cryst}\delta\phi_{micro}/\delta T], \quad (7b)$$

in which and E_r, ρ_{lava} and L_{cryst} are the effusion rate, density, and latent heat of crystallization, respectively (see Tables 1, 2, 3). In other words, for a given effusion rate (E_r) and crystallization rate ($\delta\phi_{micro}/\delta T$), the control volume will cool at a rate of $\delta T/\delta x$ due to the combined heat losses and gains.

Vesicularity (ρ_{lava}, cp_{lava}, α_{lava})

We account for vesicularity because of its effects on lava density, specific heat capacity, and conductivity (e.g., Robertson and Peck 1974; Wright and Okamura 1977; Peck 1978; Keszthelyi 1994). Our values for these three parameters are therefore corrected using average values for vesicularity published in Wilmoth and Walker (1993), Cashman et al. (1994), and Gaonac'h et al. (1997).

Surface thermal structure (f_{crust}, T_{crust}, T_{hot})

To estimate the surface heat fluxes Q_{rad}, Q_{force}, and Q_{rain}, the thermal structure of the lava surface must be known. Following Crisp and Baloga (1990), our heat budget model assumes a lava surface composed of two thermal components: a chilled crust at temperature T_{crust} occupying fraction f_{crust} of the surface, and areas where molten lava at a much higher temperature (T_{hot}) is exposed. This high temperature lava (T_{hot}) occupies the remaining surface fraction ($f_{hot}=1-f_{crust}$). Note that T_{hot} is not the same as, and is always less than, the core temperature (explained below).

Fractional crust coverage

Field observations show that disruption of the chilled crust and consequent exposure of hotter lava is a function of flow velocity (Lipman and Banks 1987; Rowland and Walker 1990). This function is, however, yet to be rigorously quantified. One exception is the range of f_{crust} values from 0.4 to 0.8 measured by Flynn and Mouginis-Mark (1994) at an active lava channel on

Table 3 Heat budget terms. See Tables 1 and 2 for definition of constants and variables

Term	Definition	Derivation of flux in W m^{-1}
Q_{rad}	Radiative heat loss	$Q_{rad}=\sigma\varepsilon[f_{crust}T_{crust}^4+(1-f_{crust})T_{hot}^4]w$
Q_{force}	Forced convection	$Q_{force}=UC_H\Delta T_{surf}\rho_{air}cp_{air}w$
Q_{free}	Free convection	$Q_{free}=0.14\alpha_{air}(g\kappa_{air}\rho_{air}/\eta_{air}\beta_{air})^{1/3}(T_e-T_{air})^{4/3}w$
Q_{rain}	Heat loss by rain vaporization	$Q_{rain}=\delta R/\delta t\rho_{H2O}L_{H2O}w$
Q_{cond}	Conductive heat loss	$Q_{cond}=\alpha_{lava}(\Delta T_{base}/H_b)w$
Q_{cryst}	Heat from crystallization	$Q_{cryst}=\delta T/\delta xE_r\rho_{lava}L_{cryst}\delta\phi_{micro}/\delta T$
Q_{visc}	Heat from viscous dissipation	For semi-circular channel $Q_{visc}=\eta(V/w)^2d$ Where w>d $Q_{visc}=\eta(V/d)^2w$

Kīlauea (Hawai'i) that had a surface velocity of ~2 m s^{-1} (L.P. Flynn, pers. commun.). Examination of photographs of channelized Hawaiian flows having known velocities (Lipman and Banks 1987; Wolfe et al. 1988) suggests that the relationship between f_{crust} and V is an exponential one:

$$f_{crust} = 0.9 \exp(-0.16\,V) \quad [\text{correlation coefficient} = 0.9] \tag{8}$$

For a velocity of 2 m s^{-1} Eq. (8) gives f_{crust} of 0.65, agreeing well with the values measured by Flynn and Mouginis-Mark (1994).

Crust temperature

Hon et al. (1994) show that crusts forming on cooling pāhoehoe lobes vary as a function of time (t), where T_{crust}=ln(t/145.79)/–0.01644. For crust surfaces that are 1 s, 1 min, and 1 h old this gives T_{crust} of 800, 550, and 300 °C, respectively. Thermocouple measurements of flexible crusts on actively inflating pāhoehoe lobes at Kīlauea give T_{crust} in the range 269–682 °C (mean=535±110 °C, n=26). Multispectral measurements made by Flynn and Mouginis-Mark (1994) at the center and margins of a lava channel on Kīlauea yield T_{crust} of 736–940 °C (mean=871±57 °C, n=8), and 458–654 °C (mean=556±59 °C, n=6), respectively. Based on these data, we select a starting T_{crust} of 550± 125 °C, corresponding to a crust that is ~1 min old.

High-temperature component of the crust

Observations of channelized flows at Kīlauea and Etna show that the incandescent, hottest portions of the flow surface are typically some tens of degrees Celsius cooler than the core temperature (T_{core}; Calvari et al. 1994; Flynn and Mouginis-Mark 1994; Harris et al. 1998). Measurements made by us at a ~1-m-wide channel at Kīlauea on 11 November 1999 showed maximum surface temperatures of 1020–1055 °C across incandescent lava flowing at ~1 m s^{-1} out from under a down-flow-developing tube. Simultaneous core temperatures were 1161 °C, yielding a difference between T_{hot} and T_{core} of 106–141 °C. This difference is due to extremely rapid radiative cooling of exposed high-temperature surfaces the instant they are exposed to the atmosphere. To describe the highest temperature thermal component encountered at the lava surface, we therefore use

$$T_{hot} = T_{core} - y \tag{9}$$

in which y=0 to 140 °C. At each 1-m down-flow increment along the channel, once the thermal structure of the control volume crust is determined, Q_{rad}, Q_{force}, and Q_{rain} are calculated using the formulae presented in Table 3.

Basal crusts (H_b)

Q_{cond} is calculated from the relationship given in Table 3 using base crust temperature and thickness constraints from available field data and model results. Keszthelyi (1995b) and Wooster et al. (1997) show that T_{base} is typically 700±200 °C. Following the cooling relationships of Hon et al. (1994), the basal crust at an inflating paāhoehoe lobe is not expected to reach 10% of the total lobe thickness until ~45 h after emplacement, and represents 1–3% of the total thickness during the first 60 min of following emplacement. 'A'ā basal crusts, however, have a different mode of formation than pāhoehoe basal crusts, typically being formed by the flow overrunning clinker which has tumbled from the flow front rather than by conductive thickening, although some thickening by conductive cooling must also occur. As a result, we expect 'a'ā basal crusts to be thicker than those at pāhoehoe flows, and indeed our observations of 'a'ā outcrops on Stromboli, Etna, and Hawai'i show that layers of basal clinker typically make up ~10% of the total flow thickness. We use a base crust thickness (H_b) which is 10% of the total flow thickness.

Viscous dissipation (Q_{visc})

Viscous dissipation is heat generated by internal friction when a fluid flows. Note from the viscous dissipation formulae in Table 3 that this heat-gain term has a direct relationship with viscosity and the square of velocity; however, viscosity and velocity have an inverse relationship with each other (Eqs. (2a), (2b)). As is discussed below, Q_{visc} turns out to be negligible.

Running the model

FLOWGO advances a control volume of lava down the channel in a 1-m increment and using the relationships given above, determines the total heat loss and gain. At the end of that increment FLOWGO adapts the control volume by reducing T_{core} (and hence T_{hot}) and T_{crust} by $\delta T/\delta x$. The new temperatures and consequent ϕ_{total} are then used to recalculate all temperature and crystallinity dependent variables, some of which are interrelated with each other. These are V (which also varies depending on the slope beneath the increment), η, YS_{core}, YS_{base}, Q_{rad}, Q_{force}, Q_{rain}, Q_{cond}, Q_{cryst}, Q_{visc}, and f_{crust}, as well as H_s (see Appendix). These adapted values are used to determine cooling across the next 1-m increment, and so on down channel. Thus, as the control volume advances numerous interrelated effects occur: (a) as long as velocity drops, a surface crust of increasing extent and thickness and decreasing temperature develops; (b) the core cools

Table 4 Summary of the steps executed by FLOWGO and FLOWGO(B). These steps are executed by the FLOWGO program sequentially in the order given

Step	Description	Source
1	Set and/or calculate all input parameters for lava leaving the vent and correct parameters for vesicularity	Tables 1, 2, 3
2	Select slope model: read from DEM or user input slope segments	Fig. 5
3	Calculate viscosity as a function of temperature and crystallinity for this segment of the flow	Eq. (3)
4	Calculate yield strength as a function of temperature and crystallinity for this 1-m-long segment of the flow	Eq. (4a, 4b)
5	Set slope for this portion of the flow, where slope is variable with distance down-flow	Fig. 5, Table 2
6	Calculate flow velocity as a function of channel depth/radius, yield strength, density, viscosity and slope down this segment of the flow	Eq. (2a, 2b)
7	Calculate fractional crust coverage as a function of velocity for this segment of the flow	Eq. (8)
8	Calculate Reynolds number (Re), effective radiation temperature for this segment and during the first iteration, the at-vent effusion rate (E_{vent}). In subsequent runs, conserve volume by varying channel width (w), so that $w=E_{vent}/(d\ V)$ and $E_r=E_{vent}$ at all points down-flow	$Re=[4\rho_{lava}(w/3)V]/\eta$ Table 2
9	Calculate radiative heat loss per unit length	Table 3
10	Calculate convective heat loss per unit length	Table 3
11	Calculate heat loss due to rain per unit length	Table 3
12	Calculate crustal thickness from the surface heat losses and then crust survival time using calculated crust thicknesses and effusion rate	Appendix
13	Calculate conductive heat loss per unit length	Table 3
14	Calculate heat loss per unit length due to entrainment of crustal material (optional)	Appendix A
15	Calculate heat gain due to crystallization per unit length	Table 3
16	Calculate heat gain due to viscous dissipation per unit length	Table 3
17	Calculate the cooling rate over this 1-m-long segment of the flow	Eq. (7a, 7b)
18	Decrease all lava temperatures by the cooling rate over this 1-m-long segment of the channel to obtain the input temperatures for the control volume in the next segment	
19	Calculate down-channel increase in crystallinity within the control volume as a function of the temperature change over the next 1 m length of the flow	Eqs. (5a, 5b), (6a, 6b)
20	Calculate distance down-flow (DIST) that the control volume has reached	=DIST+L
21	Calculate the amount of time that it has taken the control volume to reach this distance down-flow from the vent	=V/DIST
22	IF V>0 AND $T_{core}>T_{solid}$ Then advance the control volume 1 m and repeat steps 3–21 using the new temperatures calculated in step 18 Otherwise end	
23	Output down-flow crustal, thermal, and rheological parameters, plus final channel length and at-vent effusion rate. Down-flow thermal and rheological parameters can be put out every *N* meters, where *N* is the sampling interval input by the user	

but that heat loss is modulated by latent heat of crystallization; (c) yield strength and viscosity increase; (d) velocity drops unless there is an increase in the underlying slope; and (e) the channel widens or narrows to conserve mass as velocity varies. As long as velocity is greater than zero and/or T_{core} is greater than solidus (T_{solid}), the new heat content terms are used to determine a new cooling rate and a new iteration starts for the next meter increment. The point at which V=0 and/or $T_{core}=T_{solid}$ gives the maximum distance that our control volume can extend. This iterative process is summarized in Table 4.

FLOWGO is written in Interactive Display Language and allows model variables to be input and modified by the user so that they can be set to those applicable to the eruption under consideration. Values used by us for the Mauna Loa 1984 flow are given in Tables 1 and 2. We allow for variations in topography by either splitting the downhill path into *n* segments of defined slope or by reading a two-column ASCII file containing slopes at defined downhill distances, with FLOWGO interpolating between the slopes of the nearest two points.

Results and validation

Input constants and variables used in the three test cases considered here are given in Tables 1 and 2. To constrain variation in results we defined two combinations of input parameters using a reasonable, error-defined range of values. These combinations produce rapid and slow heat-loss end members (termed the hot and cool models, respectively; Table 5). The hot model has high-temperature crusts, high vesicularity, and a low phenocryst content, and in the figures herein is always represented by a solid line. The cool model has lower-temperature crusts, low vesicularity, and high phenocryst content, and is represented by a dashed line. The range of solutions obtained using these end-member models give the upper and lower bounds of our expected error. Unless otherwise stated, results herein give the range of solutions bounded by these two models, with the hot model result always presented first.

Table 5 Summary of the hot and cool end-member models used to run FLOWGO, with input parameters used in our simulations of the Mauna Loa 1984, Pu'u 'Ō'ō 16 May 1997, and Etna 11–12 October 1998 flows

Parameter	Model		Mauna Loa[b]		Pu'u 'Ō'ō[c]		Etna[d]	
	Cool	Hot	Cool	Hot	Cool	Hot	Cool	Hot
w			5.5 m	5.5 m	5.0 m	5.0 m	5.0 m	5.0 m
d			5.5 m	5.5 m	3.0 m	3.0 m	1.25 m	1.25 m
	Cool:	Hot:						
T_{air}	Min. T_{air}	Max. T_{air}	10 °C	30 °C	10 °C	30 °C	−10 °C	0 °C
T_{erupt}	Min. T_{erupt}	Max. T_{erupt}	1137 °C	1143 °C	1150 °C	1150 °C	1080 °C	1090 °C
T_{solid}	Min. T_{solid}	Max. T_{solid}	970 °C	990 °C	970 °C	990 °C	970 °C	990 °C
	High crystallinity	Low crystallinity						
ϕ_{phen}[e]	Max. ϕ_{phen}	Min. ϕ_{phen}	0.15	0.00	0.00	0.00	0.34	0.27
ϕ_{post}			0.45	0.45	0.45	0.45	0.41	0.41
	Cool crust:	Hot crust:						
T_{crust} (av)	Min. T_{crust}	Max. T_{crust}	425 °C	675 °C	425 °C	675 °C	425 °C	675 °C
T_{hot}[a]	Min. T_{hot}	Max. T_{hot}	y=140	y=0	y=140	y=0	y=140	y=0
T_{base}	Min. T_{base}	Max. T_{base}	500 °C	900 °C	500 °C	900 °C	500 °C	900 °C
	Thick base:	Thin base:						
H_b	Max. H_b	Min. H_b	19%	1%	19%	1%	19%	1%
	Dense:	Vesicular:						
Ves	Min. vesicularity	Max. vesicularity	1%	15%	23%	23%	13%	25%

[a] T_{hot}=T_{core}−y (Eq. 9)
[b] See Table 2 for parameter source/derivation for Mauna Loa, where we use a vesicularity of 8±7% calculated from density data in Lipman and Banks (1987)
[c] All input parameters for Pu'u 'Ō'ō are taken from Cashman et al. (1999)
[d] Etna flow dimensions and air temperatures are taken from our field measurements and T_{erupt} from the core temperature of 1085±5 °C given in GVN (1999b). Crystallinities for Etna are set using ϕ_{phen} of 34±7% and ϕ_{post} of 41% calculated from data in Tanguy and Clocchiatti (1984), Armienti et al. (1984, 1990, 1994), Tanguy (1973), Tonarini et al. (1995), and Ryan and Sammis (1981). A vesicularity of 19±6% is calculated from Etna 'a'ā vesicularity data given by Gaonac'h et al. (1997)
[e] For the Pu'u 'Ō'ō flow, because vent samples were nearly aphyric (Cashman et al. 1999), we use 0% phenocrysts for both models
(av) At-vent starting temperature

Viscosity and yield strength

In line with Murase and McBirney (1973) and McBirney and Noyes (1979), modeled viscosities and yield strengths are heavily dependent on the concentration of solids (Figs. 5, 6, 7). In all three test cases, FLOWGO produces a steady increase in viscosity over most of the flow, with values typically in the range of 10^3–10^4 Pa s (Fig. 6). This is consistent with Murase and McBirney (1973) and Shaw et al. (1968) who give a viscosity of 10^3–10^4 Pa s for basalt at ~1100 °C, and with Pinkerton and Sparks (1978) who obtained a viscosity of 9400±1500 Pa s for basaltic andesite 3 m down-flow from an active vent on Etna. For the Mauna Loa case, hot model runs with starting phenocryst contents (ϕ_{phen}) of 0–15% and cool model runs with 15% phenocryst contents both give viscosities that approximate those calculated for this flow by Moore (1987; Fig. 6a).

When ϕ_{phen}=0 (i.e., the lava is aphyric upon eruption), modeled yield strength approaches zero near the vent. The presence of phenocrysts, however, results in modeled near-vent yield strengths of 10–10^2 Pa, and in all cases modeled yield strengths increase rapidly at the distal end (Fig. 7). In the Mauna Loa case this increase is particularly sudden after 5–25 km of slowly increasing yield strength. Yield strengths calculated for the 1984 Mauna Loa flow by Moore (1987) are 146±63, 922±424, and 2333±306 Pa at distances of 4, 10, and 15 km from the vent, respectively. We can approximate these values at these distances by running FLOWGO with ϕ_{phen}=15–30% (Fig. 7a), but these runs do a poor job of replicating the channel length. We therefore prefer hot model runs with ϕ_{phen} =0% and cool runs with ϕ_{phen}=15%. Using these values, over a temperature drop of 70 °C, FLOWGO produces yield strengths of 95–273 and 60–70 Pa, respectively, for the Mauna Loa and Pu'u 'Ō'ō cases. These results agree with the data of Shaw et al. (1968) who measured yield strengths of 70–120 Pa for lava cooling ~70 °C below its liquidus at Makaopuhi lava lake (Kīlauea). For comparison with FLOWGO, in Fig. 7 we plotted this yield strength given by Shaw et al. (1968) at the modeled down-channel distance where T_{core} has dropped by 70 °C. At Etna the hot model produces yield strengths of 140±80 Pa at temperatures of 1086±3 °C, which compare with yield strengths of 370±30 Pa obtained for Etnean lavas at 1086±3 °C by Pinkerton and Sparks (1978).

Channel dimensions, velocity, effusion rate, volume, and emplacement duration

Using input values given in eruption accounts we are able to closely reproduce actual dimensional and

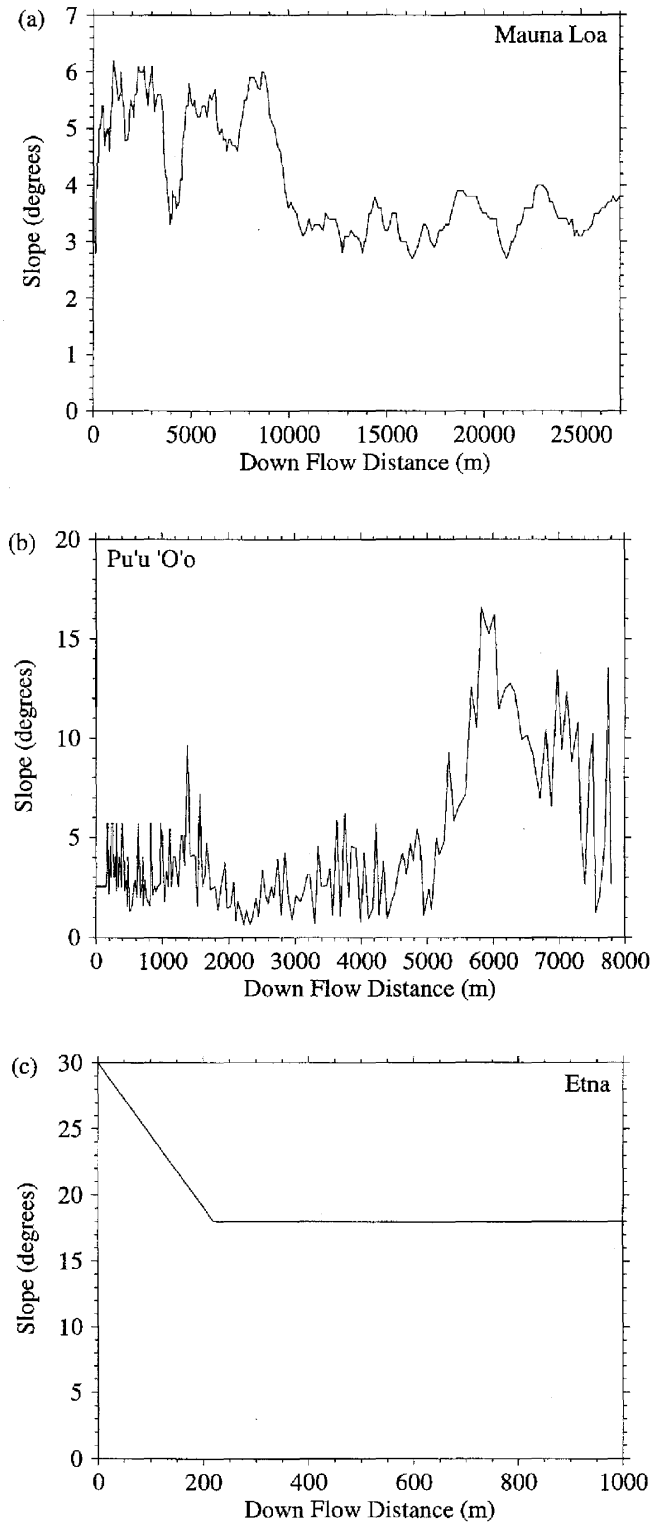

Fig. 5 Variation in slope down the channel center line for the modeled cases at **a** Mauna Loa, **b** Pu'u 'Ō'ō, and **c** Etna

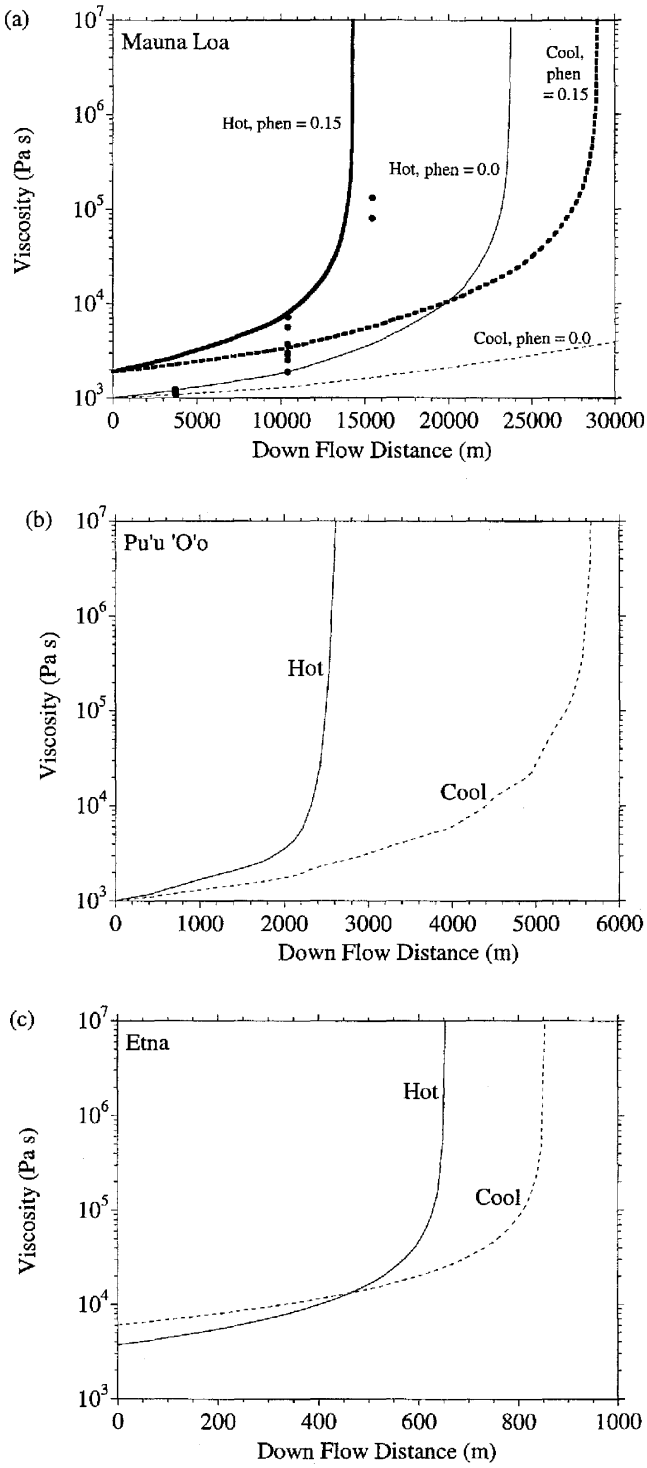

Fig. 6 Down-flow variation in viscosity given by FLOWGO for the hot (*solid line*) and cool (*dashed line*) cases at **a** Mauna Loa, **b** Pu'u 'Ō'ō, and **c** Etna. For comparison, viscosities obtained for the Mauna Loa flow by Moore (1987) are also given (*dots*). For Mauna Loa the hot and cool models have been run using phenocryst mass fractions of 0.0 (*thin lines*) and 0.15 (*thick lines*)

velocity values. Our Mauna Loa simulation gives a channel that is 24–29 km long, in comparison with field-derived flow lengths of 25 and 27 km (flows 1 and 1b; Fig. 2). Modeled channel widths also compare

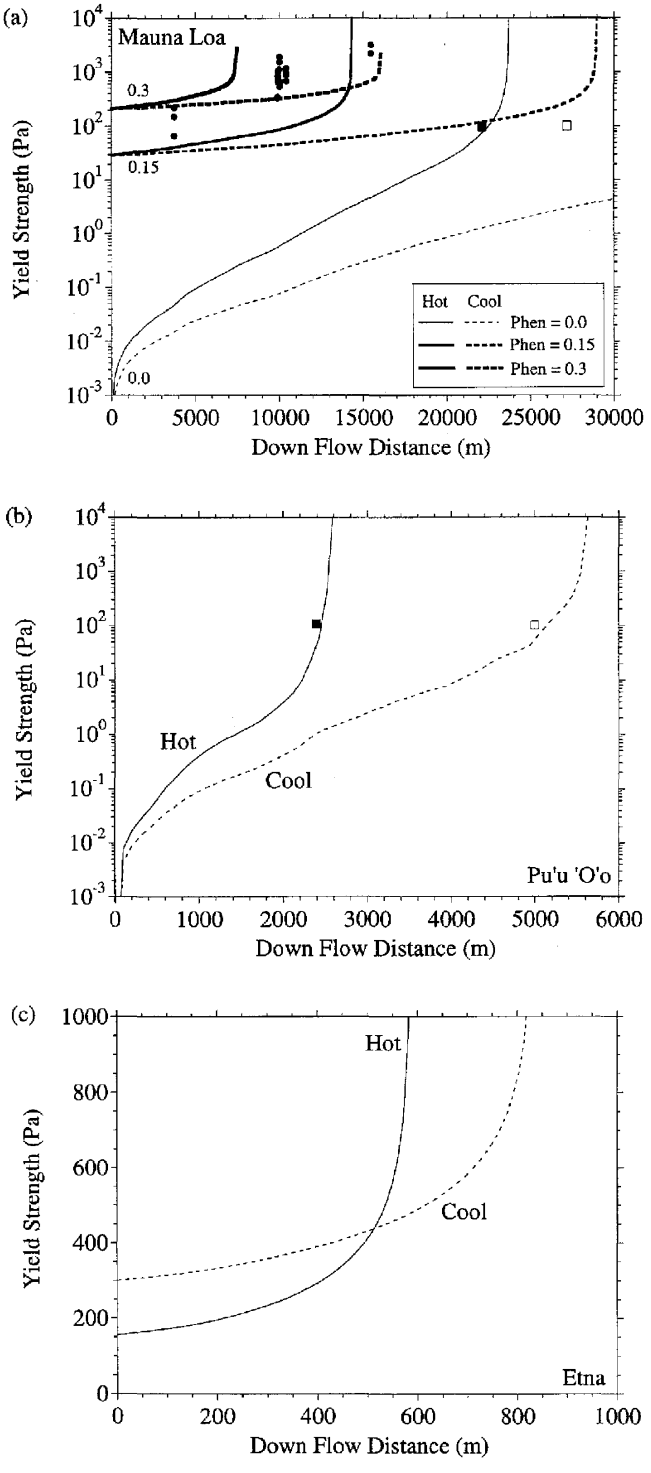

Fig. 7 Down-flow variation in yield strength given by the hot (*solid line*) and cool (*dashed line*) modeled cases at **a** Mauna Loa, **b** Pu'u 'Ō'ō and **c** Etna. The Mauna Loa models have been run with a range of phenocryst mass fractions from 0 (*thinnest line*) to 0.3 (*thickest line*). For comparison, yield strengths obtained for the Mauna Loa flow by Moore (1987) are given (*dots*). Yield strengths for a Kīlauea tholeiite after 70 °C cooling were determined by Shaw et al. (1968) and are plotted at the down-flow distance at which the core in the hot and cool models has cooled by 70 °C (*solid and open squares*, respectively)

well with field measurements (Fig. 8a). Our control volume takes 9–22 h to travel from the vent to the distal end, consistent with Crisp and Baloga (1994) who use velocity estimates of Lipman and Banks (1987) to suggest that the time taken for a lava batch to reach 27 km from the vent was ~24 h.

We obtain an effusion rate of 660–400 $m^3 s^{-1}$, which compares with field-based estimates of 806–278 $m^3 s^{-1}$ during the first few days of the eruption (Lockwood et al. 1985; Lipman and Banks 1987; Moore 1987). During the course of this eruption, however, declining effusion rates were reflected in reduced channel velocities. Effusion rates peaked at 806 $m^3 s^{-1}$ during the first 6 h, and declined to a relatively stable 139–278 $m^3 s^{-1}$ over the next 12 days, before declining farther (Lipman and Banks 1987). This was accompanied by declining channel velocities which, at 0.5 km from the vent, fell from 15.0–17.8 m s^{-1} at the start of the eruption to 1.25–6.45 m s^{-1} around the twelfth day (Lipman and Banks 1987). Because input variables for both our hot and cool models are those that would simulate conditions early in the eruption, modeled velocities compare well with velocities measured prior to day 12 (6 April; Fig. 9a). To take into account the declining lava production rate, we run a late-stage model with the following parameters: channel depth=2.2 m; effusion rate=26 $m^3 s^{-1}$; and starting crust temperature=300 °C. These values are essentially those reported by Lipman and Banks (1987) for this late-stage activity (channel depth of 2.0 m and at-vent effusion rate of 28 $m^3 s^{-1}$). We also used an iteratively derived crustal growth model, $f_{crust}=\exp(-0.00756\ V)$, which accounts for the more extensive crust during the later stages of the eruption. FLOWGO results using these late-stage parameters agree well with field observations late in the eruption (Fig. 9a).

At Pu'u 'Ō'ō FLOWGO produces a 2.5- to 5.7-km-long channel, compared with a reported flow length of 4 km (Cashman et al. 1999). Over the first half of the Pu'u 'Ō'ō flow, we obtain mean channel width and velocity of 6–10 m and 2.3–1.9 m s^{-1} (Figs. 8b, 9b), compared with field-based values of 5–10 m and 1–2 m s^{-1} (Cashman et al. 1999). FLOWGO-derived effusion rates of ~39 $m^3 s^{-1}$ agree with 37.5± 22.5 $m^3 s^{-1}$ calculated from channel dimensions and velocities given in Cashman et al. (1999) and 20±7 $m^3 s^{-1}$ calculated by Blake (in press).

For Mt. Etna, we obtain a 590- to 830-m-long channel, compared with a field-measured flow length of 755 m. Average modeled channel width (21 m; Fig. 8c) compares with an actual channel width range of 10–30 m (Fig. 3). Modeled maximum and average velocities are 1.34–0.95 m s^{-1} and 0.51–0.35 m s^{-1}, respectively (Fig. 9c), yielding an effusion rate and total DRE volume of 8.4–6.0 $m^3 s^{-1}$ and 0.4–0.5×10^5 m^3. Our field-derived DRE volume is 0.5± 0.3×10^5 m^3.

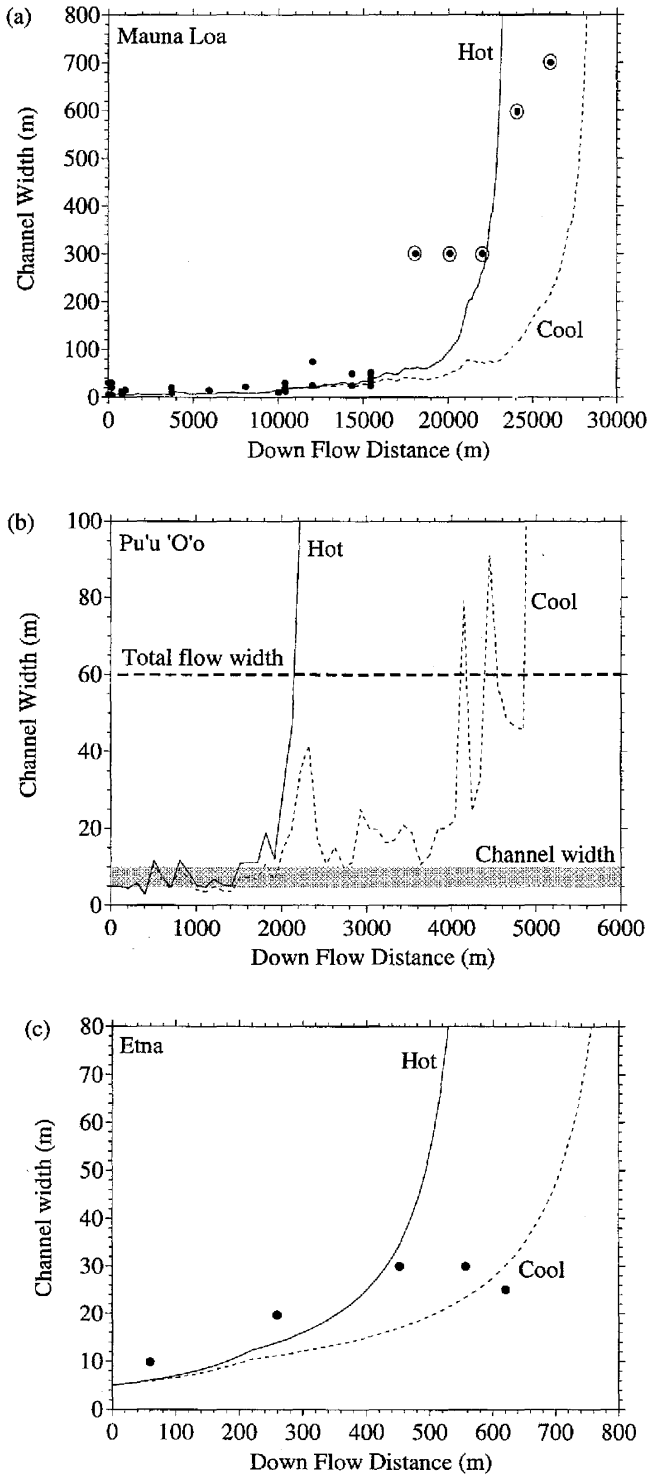

Fig. 8 Down-flow variation in channel width given by the hot (*solid line*) and cool (*dashed line*) modeled cases at **a** Mauna Loa, **b** Pu'u 'Ō'ō, and **c** Etna. For comparison, channel and flow widths (*black and ringed black circles*, respectively) for the Mauna Loa flow from Lipman and Banks (1987), for Pu'u 'Ō'ō from Cashman et al. (1999; *gray zone*), and for Etna from our field mapping (*black circles*) are given. Lipman and Banks (1987) width data beyond 16 km are total flow widths and the *horizontal dashed line* in **b** gives the channel plus levee width from Cashman et al. (1999). Note that near the flow front the channel becomes less distinct, defined only by shear-zones. Thus the modeled channel width begins to approach the total width in distal portions of the flow

The down-flow heat budget

Over the majority of the flow length Q_{rad} is typically 10^5–10^6 W m^{-1} and accounts for 70–90% of the total heat loss (Fig. 10). Q_{force} and Q_{cond} are 10^4–10^5 W m^{-1} and each account for between 1 and 15% of the total heat loss. The relative values of the surface and basal temperatures determines whether $Q_{force}>Q_{cond}$. The different input eruption temperatures (and hence T_{hot}; Table 5) result in $Q_{force}>Q_{cond}$ at Mauna Loa and Pu'u 'Ō'ō but $Q_{force}<Q_{cond}$ at Etna (Fig. 10). The lower eruption temperature and T_{hot} at Etna also somewhat equalizes Q_{rad}, Q_{force} and Q_{cond} to 65–75, 10–15 and 15–20% of the total heat loss, respectively. Heat losses due to rain are typically $<10^4$ W m^{-1} and in comparison to other heat losses are trivial (Fig. 10). Along most of the flow Q_{cryst} accounts for >90% of the heat gained by the control volume, with typical values of 10^5–10^6 W m^{-1} (Fig. 11). Q_{visc} is typically 10^3–10^5 W m^{-1}.

Modeled down-flow cooling and crystallization

We concentrate our cooling and crystallization checks on the Mauna Loa and Pu'u 'Ō'ō cases because we have no field temperature or crystallinity data for the Etna case. In the vent-proximal channel, we model Mauna Loa core cooling at 1.9–0.8 °C km^{-1}, compared with a cooling rate of 0.6–0.2 °C km^{-1} in the first 10 km of the Mauna Loa channel based on core temperatures measured by Lipman and Banks (1987). At Pu'u 'Ō'ō we model 11.1–3.8 °C km^{-1} compared with 6.8–4.4 °C km^{-1} measured by Cashman et al. (1999) over the first 2 km of the flow (Fig. 12b).

Recall from Eq. (9) that T_{hot} is offset from T_{core} by 0–140 °C. At the flow front, this gives T_{hot} of 990–830 °C, which compares with 900–700 °C measured by L.P. Flynn (in preparation) at incandescent cracks between the clinker on an active 'a'ā flow front. Modeled temperatures of the cool crust component (T_{crust}) decline abruptly to 540–260 °C at the flow toe at both Mauna Loa and Pu'u 'Ō'ō (Fig. 12). This compares with crust temperatures of ~300 °C obtained by L.P. Flynn (in preparation) for the surface of an 'a'ā flow a few meters behind the flow front.

The modeled down-flow increase in the volume fraction of microlites also agrees with down-flow trends in field data as well as other crystallization models (Fig. 13). FLOWGO-derived crystallization rates for the proximal-to-medial portions of the Mauna Loa and Pu'u 'Ō'ō flows are 0.002–0.01 and 0.02–0.06 volume fraction per kilometer (Figs. 14, 15),

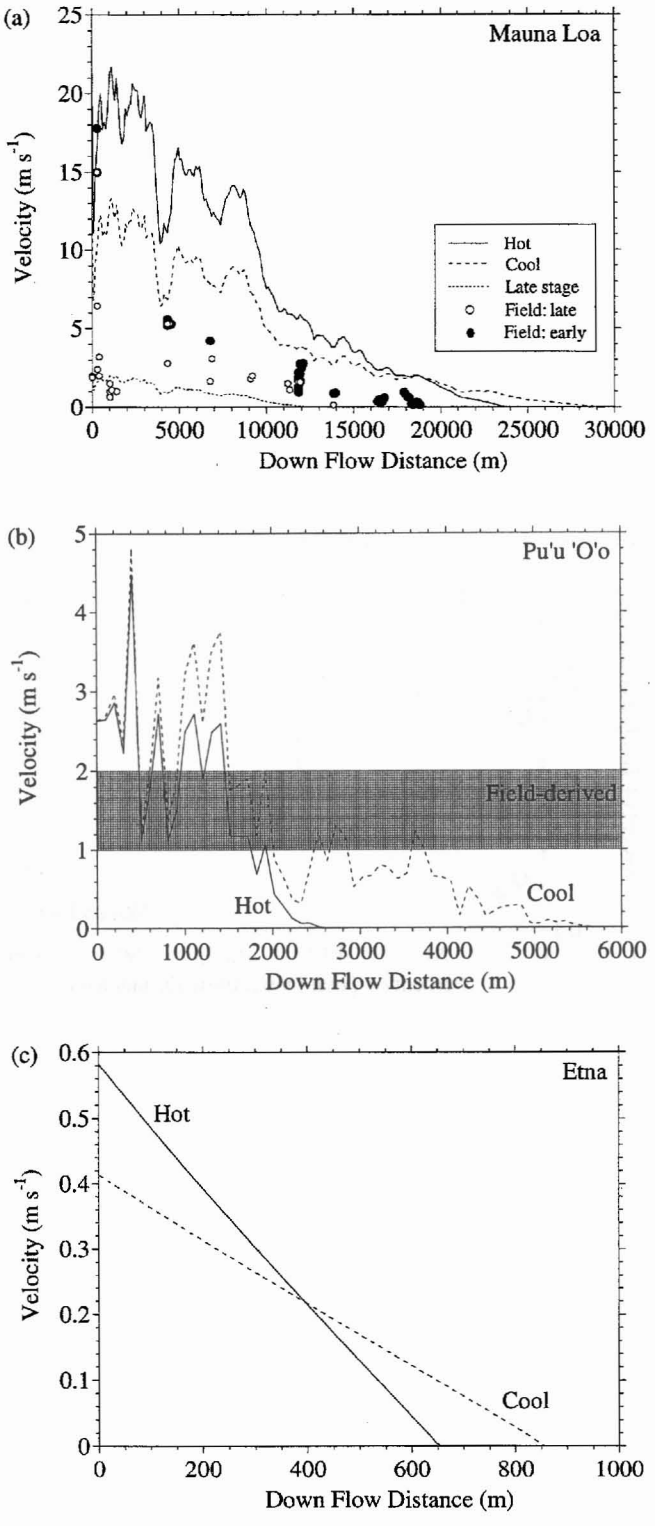

Fig. 9 Down-flow variation in velocity given by the hot (*solid line*), cool (*dashed line*), and late-stage (*dotted line*) modeled cases at **a** Mauna Loa, **b** Pu'u 'Ō'ō, and **c** Etna. Velocities for the Mauna Loa flow from Lipman and Banks (1987) are given, where *solid* and *open circles* identify early- and late-stage velocities, respectively. Velocities estimated by Cashman et al. (1999) for Pu'u 'Ō'ō (*gray zone*) are also given

compared with field-based crystallization rate estimates of 0.01–0.05 and 0.05–0.08, respectively (Crisp et al. 1994; Cashman et al. 1999). We input FLOWGO-derived cooling values into the MELTS program (Ghiorso and Sachs 1995) as an additional check on calculation of total mass solidified, and this produces crystallization rates of 0.01–0.04 and 0.06–0.22 volume fraction per kilometer, for the two cases, respectively (Fig. 14).

Over proximal portions we calculate cooling and crystallization rates of 1–10 °C km^{-1} and 0.001–0.01 volume fraction per kilometer, with viscosities and yield strengths of 10^3–10^4 and 10^{-3}–10^2 Pa s, respectively. An increase in cooling and crystallization to >100 °C km^{-1} and 0.1 volume fraction per kilometer in distal parts of the flow cause viscosity and yield strength to increase to 10^6–10^7 Pa s and 10^3–10^4 Pa s, respectively. Moore (1987) suggested a viscosity of approximately 10^7 Pa s at the distal end of the 1984 Mauna Loa flow.

Sensitivity to input variables and error

To assess model sensitivity to error in the input variables, we used the Mauna Loa 1984 cool model and varied one parameter at a time while holding all other parameters constant. Variations in channel depth, vesicularity, and phenocryst content affect modeled starting velocity (V), and in turn effusion rate (E_r) and final channel length. Changing depth by 10% causes V, E_r, and final length to change by 20, 30, and 20%, respectively (Fig. 15a, b). A 10% increase in vesicularity decreases ρ_{lava} and $c\rho_{lava}$. The resultant decrease in Q_{cryst} (Table 3) and increased cooling rate (Eq. (7a, 7b)) produce ~10% decreases in channel length, V, and E_r (Fig. 16c, d). An increase in ρ_{lava} also directly increases V (Eq. (2a, 2b)). A 10% increase in ϕ_{phen} causes viscosity and yield strength to be higher, leading to a ~20% decrease in channel length and ~30% decreases in V and E_r (Figs. 15e, f).

The remaining variables affect the cooling rate but not any of the starting, at-vent channel dimensions or rheology. They therefore only influence the final channel length. Decreasing T_{hot}, T_{crust} and/or f_{hot}, or increasing f_{crust} will all enhance insulation, in turn decreasing Q_{rad} and Q_{force} (Table 3) and allowing the lava to travel farther (Fig. 16a-b). At typical lava temperatures and crust coverage (T_{hot}=900–1000 °C, T_{crust}=400–500 °C, f_{hot}=0.4–0.2, f_{crust}=0.6–0.8) variation in T_{hot} or T_{crust} by 100 °C changes channel length by 20% and 5–15%, respectively. Variation in f_{hot} or f_{crust} by 10% changes channel length by ~10–15%.

Q_{force} and Q_{cond} depend on wind speed and basal crust thickness and temperature, respectively (Table 3). Thicker, cooler basal crusts insulate better, reduce cooling, and thus increase channel length (Fig. 16c). Reduced wind speed decreases heat loss,

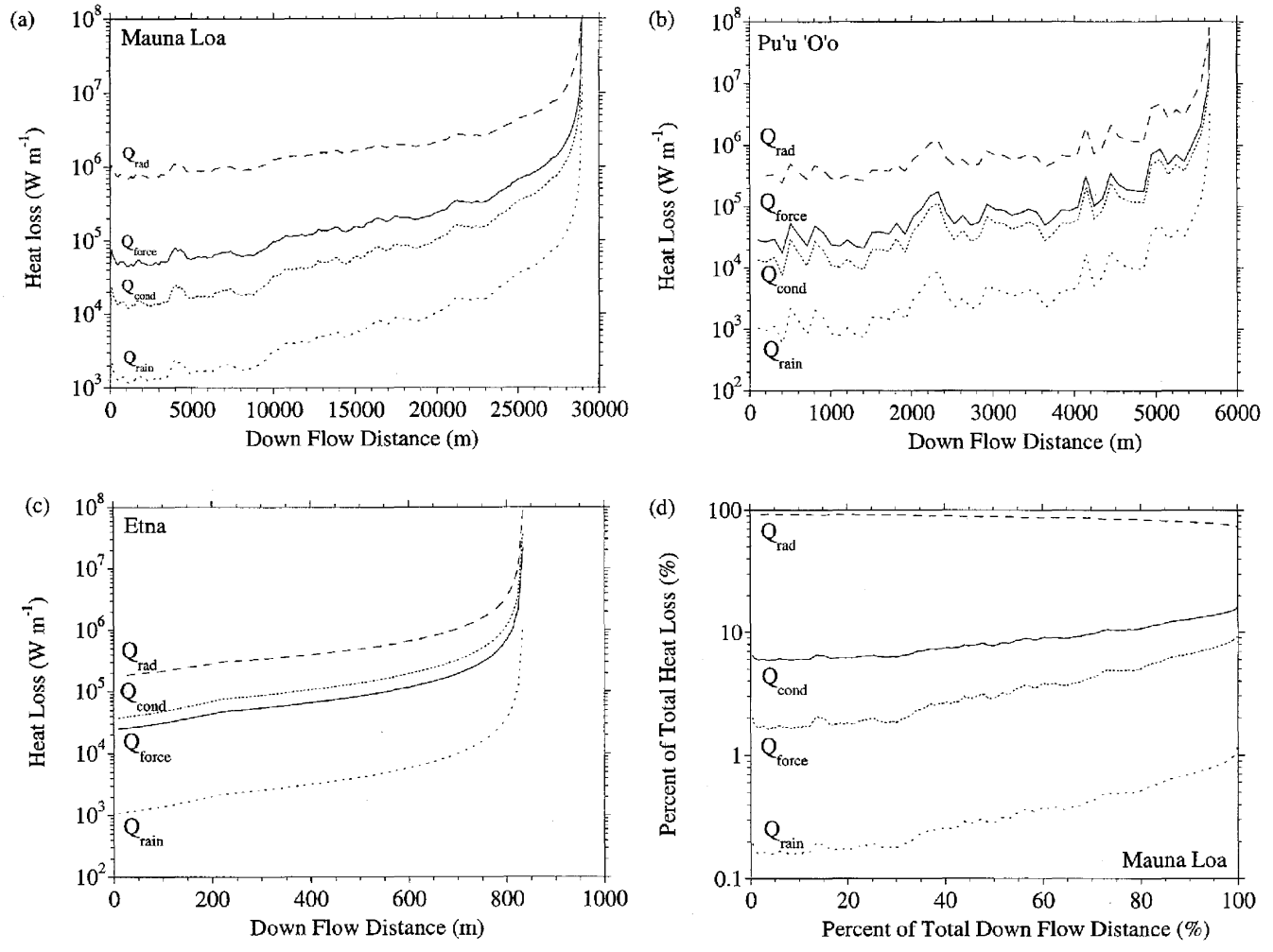

Fig. 10a–d Modeled down-flow variation in heat loss from the control volume

likewise lengthening the channel (Fig. 16d). However, the contribution of these two heat losses is less significant than that of Q_{rad} (Fig. 11), so the effects are smaller than those caused by varying the surface thermal structure. For a typical basal crust making up ~10% of the flow thickness, variation in basal temperature by 100 °C influences channel length by ~1%, with 10% variation in basal crust thickness having a similar effect. A 10% wind speed variation results in ~3% variation in channel length. Unless unreasonable rainfall rates are incorporated (and sustained over the entire history of the control volume), rain has no effect on channel length (Fig. 16e).

If the total volume fraction of microlites were higher, so would be crystallization rates (Eqs. (5a, 5b), (6a, 6b)). Within our model, this will have two opposing effects. Firstly, it will increase the rate at which viscosity and yield strength increase (Eqs. (3), (4a, 4b)) and reduce down-channel velocity (Eq. (2a, 2b)). At the same time, however, by increasing Q_{cryst} it will increase the heat supply to the control volume, counteract cooling (Eq. (7a, 7b)), and favor a longer flow. Perhaps unexpectedly the latter effect dominates in FLOWGO, meaning that a 10% increase in total microlite content results in a ~10% increase in channel length (Fig. 16f).

Discussion and conclusion

FLOWGO: advantages and improvements

We present a preliminary, self-adaptive, thermo–rheological model to describe down-flow variations in temperature, cooling, crust growth, crystallization, yield strength, viscosity, and velocity for channel-contained lava. Because our model accounts for down-channel variations in thermo-rheological parameters, it provides a better fit with field data than models which assume non-varying down-flow conditions. Figure 17 compares FLOWGO-derived temperatures with field data and modeled temperatures derived from the non-adaptive radiative-cooling model of Cashman et al. (1999). The better fit produced by FLOWGO confirms the hypothesis of Cashman et al. (1999) that

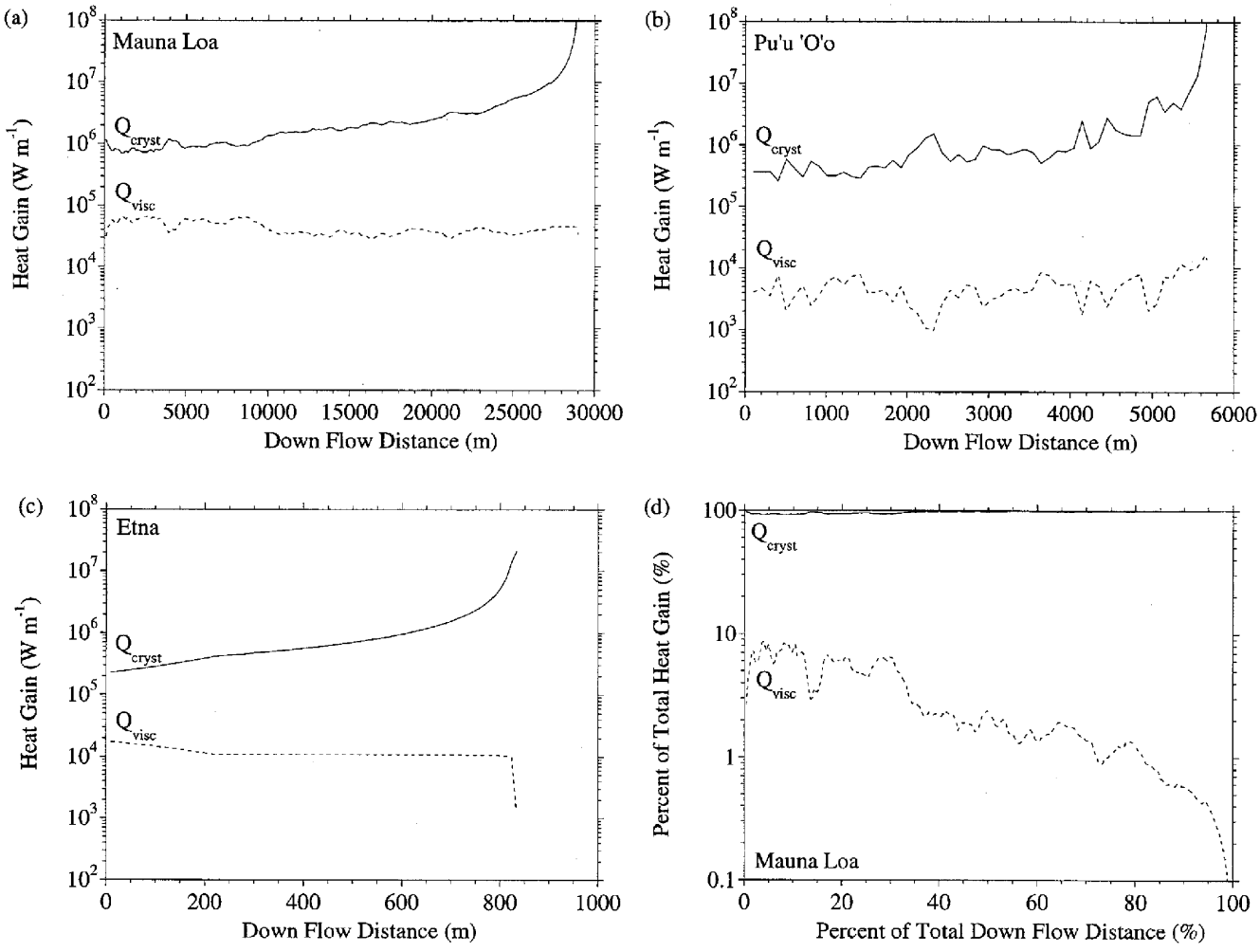

Fig. 11a–d Modeled down-flow variation in heat supply into the control volume

decreasing down-flow velocity and increasing crust cover cause a non-linear decrease in lava temperature. We also note that because crust temperature and cover are important factors in determining modeled length (Fig. 16a, b), models that do not consider the heat loss contribution of the crust will be in error. In agreement with Harris et al. (1998), our modeling also shows that heat losses due to convection and conduction are significant and should not be ignored.

Figure 17 also shows that neither the extensive-crust (late stage), cool, or the hot models can by themselves explain the entire trend indicated by the field data. Instead, the best match is obtained by a combination of the extensive-crust model in the proximal portion and cool model in the distal portion.

This is similar to our other comparisons, where some field data agree with the cool model, others with the hot model, with some falling between the two models. We therefore favor neither model, but use both together; in reality the thermo-rheological character of a flow probably switches between the two models. For example, the channel may have local constrictions not considered by our model. These may cause the crust to founder and rupture, thus causing a cool crust model to move suddenly to a hot crust model and back again. It therefore seems reasonable to assume that elements of both end-member models will be relevant at different points down the channel. In this regard, in Fig. 7 we note that in the field data a slow core cooling trend is replaced by a more rapid cooling trend at 1.2–1.6 km. This is approximately the point at which Cashman et al. (1999) report a smooth flow surface being replaced by one consisting of clinkers and broken plates.

FLOWGO is an attempt to link existing thermo-rheological models in part or in full, and allow them to draw input from, and/or provide output to, other related models. As described in this paper, because flow rheology, cooling, and crystallization involve many interrelated parameters and processes, this model is necessarily complex. We also recognize that FLOWGO is a preliminary working model subject to improvement and modification as new experimental and observational insights into rheological and heat loss processes are made. The areas where improvements can be made are described below.

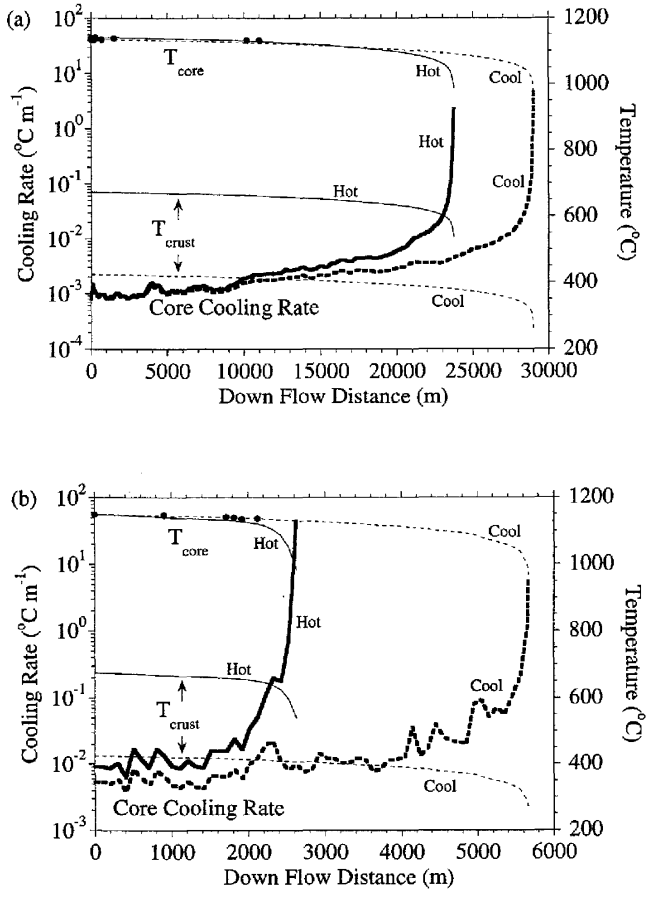

Fig. 12 Down-flow variation in cooling rate given by the hot (*thick solid line*) and cool (*thick dashed line*) models for **a** Mauna Loa and **b** Pu'u 'Ō'ō. Given on the Y2-axis are core and crust temperatures produced by the hot (*thin solid line*) and cool (*thin dashed line*) models. *Black circles* give core temperatures measured at the Mauna Loa flow by Lipman and Banks (1987) and at the Pu'u 'Ō'ō flow by Cashman et al. (1999)

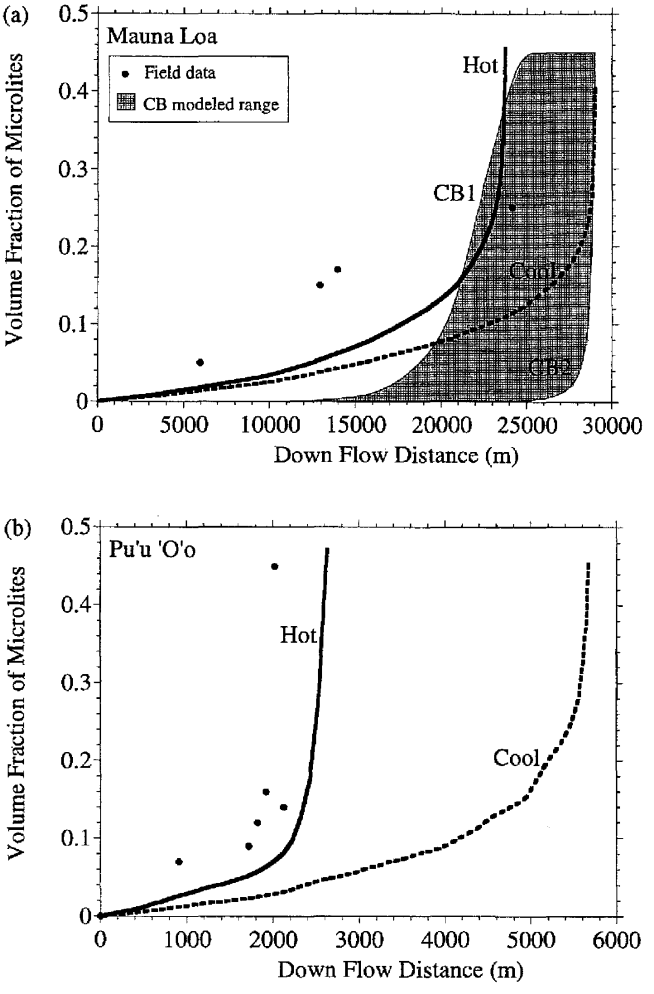

Fig. 13 Down-flow variation in volume fraction of microlites given by the hot (*thick solid line*) and cool (*thick dashed line*) models for **a** Mauna Loa and **b** Pu'u 'Ō'ō. In **a**, down-flow variation in microlite volume fraction measured for the Mauna Loa flow by Crisp and Baloga (1994) and predicted by their modeled relationship between lava travel time (here converted to distance) and microlite content are given by the *black circles* and *thin solid lines bounding gray zone*, respectively. The upper and lower limits of the Crisp and Baloga (1994) model are labeled *CB1* and *CB2*, respectively, and have been set using values in Crisp and Baloga (1994). In **b**, *black circles* give down-flow variation in microlite content obtained for the **Pu'u 'Ō'ō** flow by Cashman et al. (1999)

Entrainment

Crisp and Baloga (1994), Keszthelyi and Self (1998), and Keszthelyi et al. (2000) have developed models to assess heat loss due to quenching the core by entrainment of cool surface crust. Version B of FLOWGO includes a simple entrainment formulation (see Appendix). This allows input and variation of parameters such as crust survival time (τ) and entrained material temperature (T_{ent}), both of which are poorly known. For the 1984 Mauna Loa flow, Crisp and Baloga (1994) suggest a volumetric entrainment rate of crust equal to 1–25% of the effusion rate, and propose that τ_e (the time required to completely mix crust and core; see Appendix) varies between 2 and 15 days, representing high and low entrainment rates, respectively. Using these values with a Mauna Loa channel depth of 5.5 m and crust thickness of 0.28 m (the mean thickness obtained using the cool FLOWGO model) we obtain τ of 9000–66,000 s (2.5–18.3 days). These values plugged into the entrainment-enabled version, FLOWGO(B), produce a channel that is 25–27 km long at all modeled T_{ent} (Fig. 18). Using the minimum τ of 300 s given by Keszthelyi and Self (1998), however, yields a channel length which is too short at any T_{ent}. We agree with Crisp and Baloga (1994) when they note that insufficient data make it impossible to tightly constrain values for T_{ent} and τ_e, or indeed down-channel variation in Q_{ent}. Due to such uncertainties, we currently run FLOWGO without entrainment.

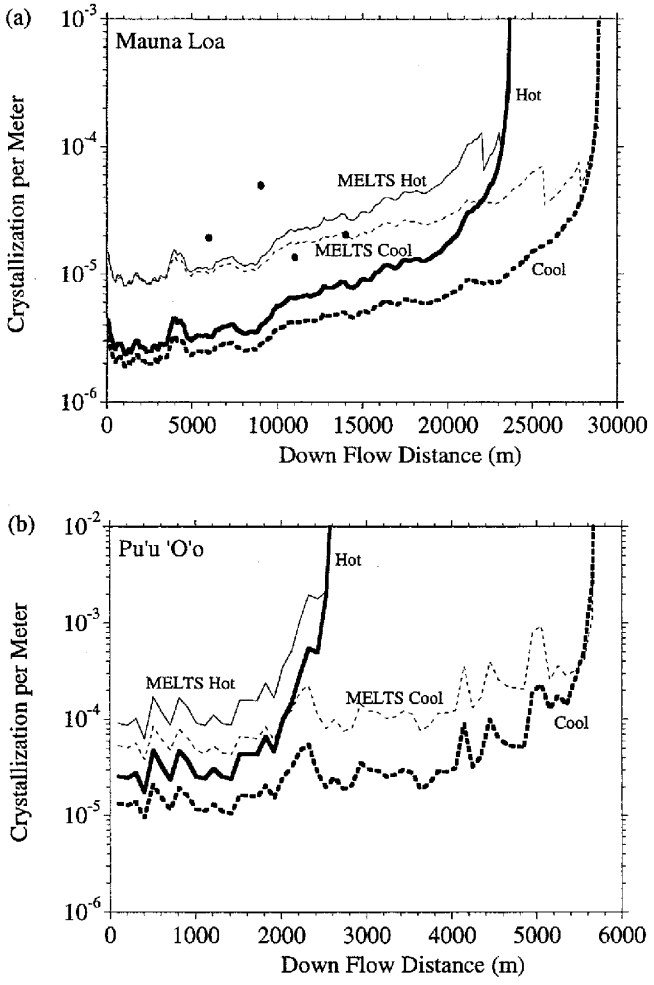

Fig. 14 Down-flow variation in crystallization rates given by the hot (*thick solid line*) and cool (*thick dashed line*) models for **a** Mauna Loa and **b** Pu'u 'Ō'ō. FLOWGO-MELTS derived crystallization rates are given by the *thin lines*. MELTS was run using a tholeiitic composition taken from Wilson (1989). Crystallization rates for the Mauna Loa flow obtained from field data by Crisp et al. (1994) are given by *black circles*

Vesicles

Although we correct all input parameters for vesicularity, we hold it constant. In reality, variable down-flow degassing has an effect on rheology, cooling, and crystallization (e.g., Sparks and Pinkerton 1978). Cashman et al. (1994) have identified down-flow variations in degassing, vesicle numbers, and sizes, Keszthelyi (1994) examined porosity effects on the transfer of heat within basaltic lava, and Mangan et al. (1998) analyzed the effect of bubbles on viscosity. Future versions of FLOWGO will take these down-flow variations in vesicle shape, number, and size into account, and consider the subsequent effects on cooling and rheology.

Crust growth and temperature

The data of Flynn and Mouginis-Mark (1994) show that crust cover and temperature evolve both down and across an active channel. Any realistic thermo-rheological model must take such variations into account because of their strong control on heat loss. However, few data on crust variations exist, and we rely on an empirical relationship between crustal coverage and velocity (Eq. (8)). Although FLOWGO results using this relationship produce good fits to field data (e.g., Fig. 17), this parameter requires refinement. Figure 17, for example, shows that the best fit to the Pu'u 'Ō'ō channel data is produced by a hybrid model, namely a crust covering 96–98% of the surface for the first ~1000 m which then breaks up and follows the velocity-dependent relationship of Eq. ((8)).

Velocity

We use the mean velocity of the control volume. Flow in a real channel is probably some form of plug flow (Cigolini et al. 1984; Lipman and Banks 1987; Moore 1987). Our use of mean velocity thus underestimates maximum velocity and overestimates the margin velocity. A more complete model must consider the full velocity profile.

Channel depth

Flow width and velocity are parameters for which field data for validation are easy to obtain. On the other hand, channel depth during an eruption is notoriously difficult to measure (e.g., Pinkerton and Sparks 1976); thus, in the current version of FLOWGO, we vary width and velocity to conserve mass, and hold depth constant. We recognize, however, that depth will also vary down-flow. Flow thickening can be calculated following Hulme (1974) from

$$d^2 = YS_{core} w/\rho_{lava}\,. \tag{10}$$

Given proximal and distal yield strengths of ~30 and ~10^4 Pa, respectively, and proximal and distal channel widths of 5.5 and 100 m, respectively, Eq. (10) yields channel depth increases between 0.1 and 6.8 m.

By re-arranging Eq. (1) and substituting into Eq. (2b) we obtain:

$$V^3 = (m^2 g \sin\theta/\rho_{lava} w^2 3\eta h)[1-(3/2)(YS_{core}/YS_{base}) + (1/2)(YS_{core}/YS_{base})^3]. \tag{11}$$

This allows us to vary velocity and depth, but with the even less reasonable requirement that channel width must be held constant. The current approach to mass conservation is a simple starting point, and there is a complex relationship between slope, velocity, width, depth, and volume loss to levees (e.g., Baloga

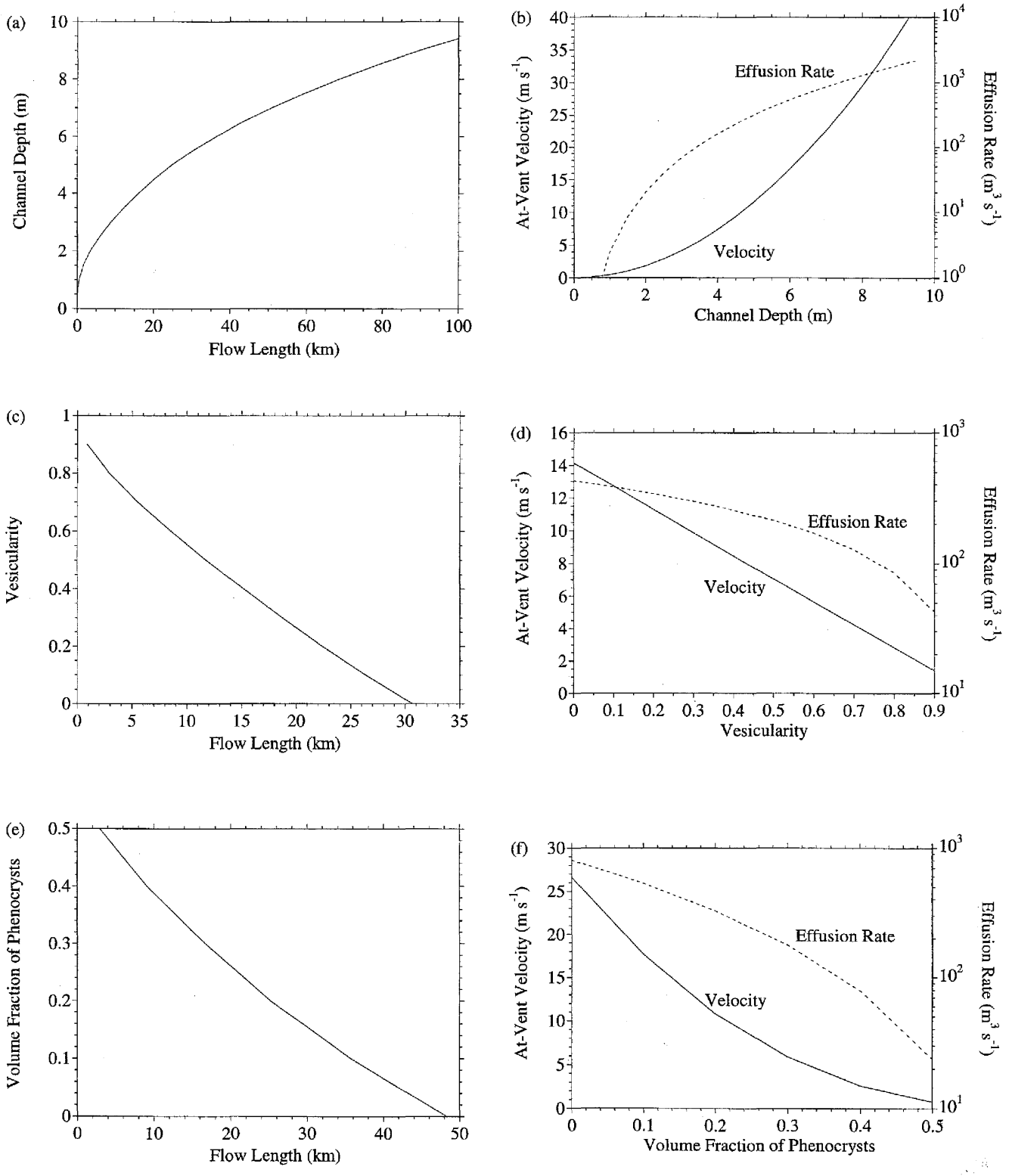

Fig. 15 **a, b** Effect of variation in channel depth on modeled length, velocity, and effusion rate. **c, d** Effect of variation in vesicularity on modeled channel length, velocity, and effusion rate. **e, f** Effect of variation in phenocryst content on modeled channel length, velocity, and effusion rate

et al. 1998). An improved model will allow variations in both width and depth, and take into account the effect of momentum and the confining effects of topography.

Regardless of the above caveats, FLOWGO does provide a starting point that outlines and links many of the primary influences on lava cooling and rheolo-

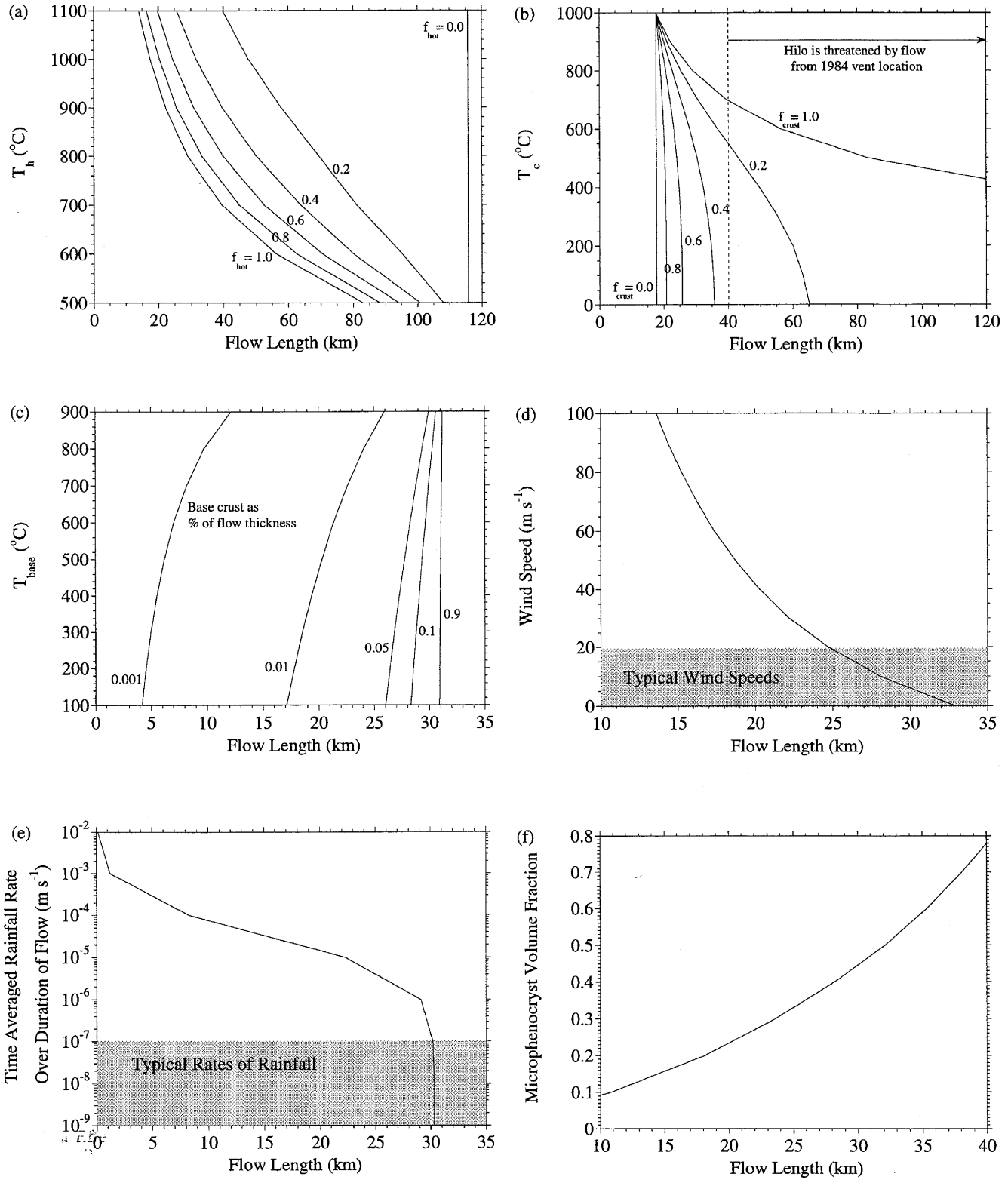

Fig. 16 **a** Effect of variation in T_{hot} and f_{hot} on modeled channel length. Results are given for a range of f_{hot} between 0 and 1. **b** Effect of variation in T_{crust} and f_{crust} on modeled channel length. Results are given for a range of f_{crust} between 0 and 1. **c** Effect of variation in T_{base} and base crust thickness on modeled channel length. Results are given for a range of base crust thicknesses between 1 and 90% of the total thickness. **d** Effect of variation in wind speed on modeled channel length. **e** Effect of variation in rainfall (time averaged over the entire duration of emplacement) on modeled channel length. **f** Effect of variation in microlite content on modeled channel length

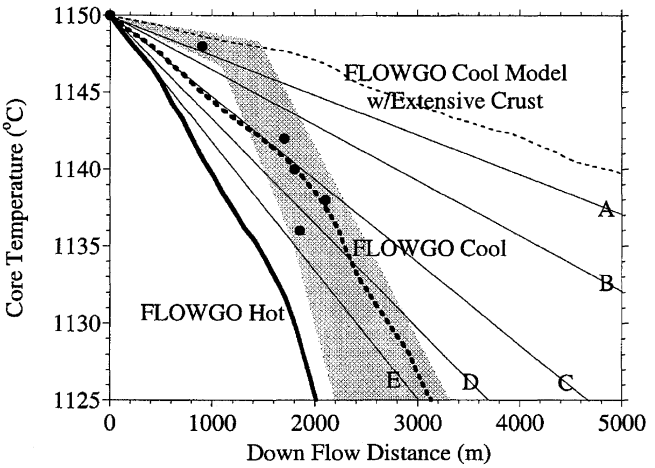

Fig. 17 Comparison between modeled and measured T_{core} at the Pu'u 'Ō'ō flow. Field measurements made by Cashman et al. (1999) are given by *black circles*. The *gray zone* indicates the field data trend. Results obtained by Cashman et al. (1999) using their radiative cooling model and a range non-varying input parameters (see Cashman et al. 1999 for details) are given by the *thin solid lines* labeled *A–E*. Results obtained using FLOWGO run using the hot and cool models for this Pu'u 'Ō'ō case are given by the *thick solid* and *dashed lines*, respectively. Result obtained using the cool model run with an extensive crust growth model [f_{crust}=exp(–0.00756 V)] is given by the *thin dashed line*

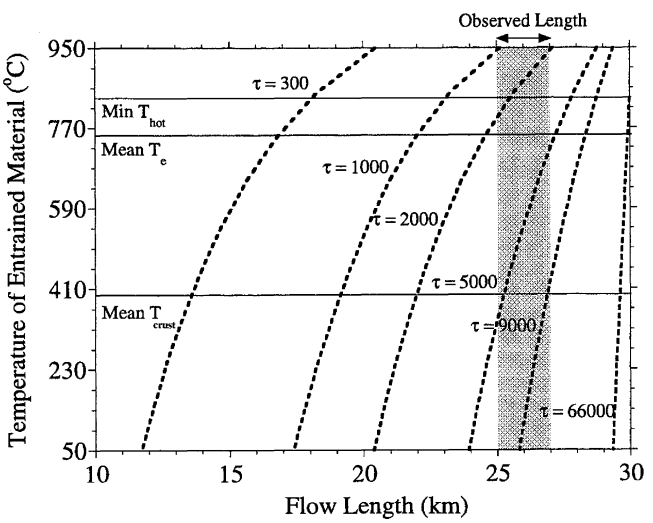

Fig. 18 Flow length produced by various combinations of T_{ent} and τ using FLOWGO(B) (see Appendix) with the cool model for the Mauna Loa 1984 flow. The *gray zone* indicates the observed flow length and *horizontal lines* indicate the mean crustal temperature, effective temperatures, and minimum T_{hot} from this cool model run. Given that any solution within or greater than the observed length is allowable, material at any temperature can be entrained as long as τ>9000 s. For τ~2000 s, T_{ent} must be greater then ~800 °C to attain the required distance. If this τ scenario applied, then only material at T_{hot} could have been entrained, and entraining material at T_{crust} would have quenched the flow to such an extent that it could not have attained the observed distance

gy. The good fit between model output and field data indicates that this preliminary model is a realistic basis from which a more complex and thorough model can evolve.

Applications: How far can a flow go?

FLOWGO allows us to determine the factors that control how far a channel can ultimately extend and potentially present a significant threat to down-flow communities. The simplest relationship is that modeled length increases with channel depth (Fig. 15a). Increasing channel depth while holding all other input parameters constant produces an increase in velocity and effusion rate. If we increase the Mauna Loa 1984 channel depth from 5.5 to 6 m, FLOWGO produces a modeled length in the 30–40 km range which could have posed a threat to the parts of Hilo directly in the flow path. However, such a flow would have required sustained effusion rates >800 m^3 s^{-1} (Fig. 15a, b), a value considerably higher than all post-contact Mauna Loa eruptions except for that of 1950 (Rowland and Walker 1990).

To increase the channel length without increasing the (already poorly constrained) channel depth, heat loss must be reduced. The most effective way to do this is to insulate the lava with a chilled crust. Covering the Mauna Loa channel with a continuous crust at ~700 °C (and holding all other input parameters constant) produces a 40-km flow (Fig. 16b), again potentially threatening Hilo. This is in agreement with Keszthelyi and Self (1998) who argue that flows do not necessarily require ultra-high effusion rates to extend >100 km and suggest that a second mechanism by which lava can flow >100 km is by insulated emplacement. Effusion rates of ~5 m^3 s^{-1} produced tube-fed pāhoehoe flows tens of kilometers long (e.g., during the 1859 and 1880–1881 eruptions of Mauna Loa), and indeed it is important to note that a continuous crust (i.e., a tube) is unlikely to develop at effusion rates >10 m^3 s^{-1} (Rowland and Walker 1990). In such cases low cooling rates of 0.35–1.8 °C km^{-1} are obtained for lava flowing in tubes (Keszthelyi 1995a; Clague et al. 1999), in comparison with 1–100 °C km^{-1} calculated here for lava in an open channel, allowing lava to advance farther before cooling forces stagnation.

Varying the thickness of the basal crust or wind speed within reasonable limits, thus changing conductive and convective heat losses, also results in channel length variation by ~15 km (Fig. 16c, d), but neither produces a flow all the way to central Hilo. Hosing the flow with water, however, would have had no effect on the final length (Fig. 16e).

In conclusion, FLOWGO is a reasonable starting point from which to analyze flow emplacement processes. It also provides a tool capable of assessing the hazard posed by hypothetical and ongoing eruptions.

Furthermore, it allows constraint of rheological and thermal regimes of flows emplaced during remote or unobserved terrestrial eruptions and in extra-terrestrial cases. The self-adaptive nature of the model means that given plausible assumptions regarding lava composition, eruption temperature, and crystal content, as well as knowing the underlying slope, we require only two inputs: at-vent channel depth and width.

Appendix: Entrainment and surface crust thickness

Following Crisp and Baloga (1994), entrainment of cooler surface crust into the hotter core causes core cooling. Including this additional heat loss term (Q_{ent}) in Eqs. (7a) and (7b) gives

$$\Delta H = -Q_{cond}-Q_{rad}-Q_{force}-Q_{rain}-Q_{ent}+Q_{cryst}+Q_{visc}$$

and

$$\delta T/\delta x = [-Q_{rad}-Q_{force}-Q_{rain}-Q_{cond}-Q_{ent}+Q_{visc}] \; [E_r \rho_{lava} L_{cryst} \delta \phi_{micro}/\delta T].$$

Following Crisp and Baloga (1994), Keszthelyi and Self (1998), and Keszthelyi et al. (2000)

$$Q_{ent} = \rho_{lava} cp_{lava} H_s (T_{core}-T_{ent})/\tau w,$$

with H_s, τ, and T_{ent} being crust thickness, survival time, and entrained material temperature, respectively. Assuming that the total surface heat loss ($=Q_{rad}+Q_{force}+Q_{rain}$) equals the heat conducted from the core across the surface crust, then H_s can be calculated from

$$H_s = \alpha_{lava}(T_{core}-T_{crust})/[(Q_{rad}+Q_{force}+Q_{rain})/w)]$$

in which α_{lava} is lava thermal conductivity. Keszthelyi and Self (1998) suggest that τ may be defined using

$$\tau = \tau_e/(d/H_s),$$

with d and τ_e being channel depth and time required to completely mix the crust with the core at any fixed point along the flow. This is obtained from Crisp and Baloga (1994)

$$\tau_e = AH_c/E,$$

in which A, H_c, and E are the control volume planimetric area, core thickness, and volume rate of entrainment, respectively. Crisp and Baloga (1994) calculate E as a function of effusion rate:

$$E = f_e E_r,$$

Acknowledgements Many thanks to S. Fagents, L. Keszthelyi, and H. Pinkerton for providing constructive reviews of a previous version of this paper, and to L. Wilson and L. Keszthelyi for discussions regarding heat loss and rheological issues. Two outstanding anonymous reviews were responsible for substantial improvements to the paper. We gratefully acknowledge L. Flynn and S. Adams for access to their unpublished data, insights, and inspiration, and to H. Garbeil for teaching FLOWGO to read slopes.

References

Archambault C, Tanguy J (1976) Comparative temperature measurements on Mount Etna lavas: problems and techniques. J Volcanol Geotherm Res 1:113–125

Armienti P, Barberi F, Innocenti F, Pompilio M, Romano R, Villari L (1984) Compositional variation in the 1983 and other recent Etnean lavas: insights on the shallow feeding system. Bull Volcanol 47:995–1007

Armienti P, Calvari S, Innocenti F, Petrini R, Pompilio M, Villari L (1990) Petrology and chemical composition. In: Barberi F, Bertagnini A, Landi P (eds) Mount Etna: the 1989 eruption. Giardini, pp 30–33

Armienti P, Clocchiatti R, D'Orazio M, Innocenti F, Petrini R, Pompilio M, Tonarini S, Villari L (1994) The long-standing 1991–1993 Mount Etna eruption: petrography and geochemistry of lavas. Acta Vulcanol 4:15–28

Baloga SM, Glaze LS, Crisp JA, Stockman SA (1998) New statistics for estimating bulk rheology of active lava flows: Puu Oo examples. J Geophys Res 103:5133–5142

Blake S (in press) Comment on Cooling and crystallization of lava in open channels, and the transition from pāhoehoe to 'a'ā. Bull Volcanol

Calvari S, Coltelli M, Neri M, Pompilio M, Scribano V (1994) The 1991–1993 Etna eruption: chronology and lava flow-field evolution. Acta Vulcanol 4:1–14

Cashman KV, Mangan MT, Newman S (1994) Surface degassing and modifications to vesicle size distributions in active basalt flows. J Volcanol Geotherm Res 61:45–68

Cashman KV, Thornber C, Kauahikaua (1999) Cooling and crystallization of lava in open channels, and the transition of pāhoehoe lava to 'a'ā. Bull Volcanol:306–323

Cigolini C, Borgia A, Castertano L (1984) Intra-crater activity, aa-block lava, viscosity and flow dynamics: Arenal volcano, Costa Rica. J Volcanol Geotherm Res 20:155–176

Clague DA, Hagstrum JT, Champion DE, Beeson MH (1999) Kilauea summit overflows: their ages and distribution in the Puna District, Hawai'i. Bull Volcanol 61:363–381

Crisp J, Baloga S (1990) A model for lava flows with two thermal components. J Geophys Res 95:1255–1270

Crisp J, Baloga S (1994) Influence of crystallization and entrainment of cooler material on the emplacement of basaltic aa lava flows. J Geophys Res 99:11819–11831

Crisp J, Cashman KV, Bonini JA, Hougen SB, Pieri DC (1994) Crystallization history of the 1984 Mauna Loa lava flow. J Geophys Res 99:7177–7198

Danes ZF (1972) Dynamics of lava flows. J Geophys Res 77:1430–1432

Dragoni MA (1989) A dynamical model of lava flows cooling by radiation. Bull Volcanol 51:88–95

Dragoni M, Tallarico A (1994) The effect of crystallisation on the rheology and dynamics of lava flows. J Volcanol Geotherm Res 59:241–252

Dragoni M, Bonafede M, Boschi E (1986) Downslope flow models of a bingham liquid: implications for lava flows. J Volcanol Geotherm Res 30:305–325

Dragoni M, Pondrelli S, Tallarico A (1992) Longitudonal deformation of a lava flow: the influence of Bingham rheology. J Volcanol Geotherm Res 52:247–254

Dragoni M, Piombo A, Tallarico A (1995) A model for the formation of lava tubes by roofing over of a channel. J. Geophys Res 100:8435–8447

Flynn LP, Mouginis-Mark PJ (1994) Temperature of an active lava channel from spectral measurements, Kilauea Volcano, Hawaii. Bull Volcanol 56:297–301

Gaonac'h H, Stix J, Lovejoy S (1997) Scaling effects on vesicle shape, size and heterogeneity of lavas from Mount Etna. J Volcanol Geotherm Res 74:131–153

Ghiorso MS, Sachs RO (1995) Chemical mass transfer in magmatic processes, IV. A revised and internally consistent thermodynamic model for the interpolation and extrapolation of liquid–solid equilibria in magmatic systems at elevated temperatures and pressures. Contrib Mineral Petrol 119:197–212
Greeley R, Iverson JD (1987) Measurements of wind friction speeds over lava surfaces and assessment of sediment transport. Geophys Res Lett 14:925–928
Gregg TKP, Fink JH (2000) A laboratory investigation into the effects of slope on lava flow morphology. J Volcanol Geotherm Res 96:145–159
GVN (1999a) Etna. Smithsonian Institution Bull Global Volcanism Network 24:3–4
GVN (1999b) Etna. Smithsonian Institution Bull Global Volcanism Network 24:6–7
Harris AJL, Butterworth AL, Carlton RW, Downey I, Miller P, Navarro P, Rothery DA (1997) Low-cost volcano surveillance from space: case studies from Etna, Krafla, Cerro Negro, Lascar and Erebus. Bull Volcanol 59:49–64
Harris AJL, Flynn LP, Keszthelyi L, Mouginis-Mark PJ, Rowland SK, Resing JA (1998) Calculation of lava effusion rates from Landsat TM data. Bull Volcanol 60:52–71
Head JW, Wilson L (1986) Volcanic processes and landforms on Venus: theory, predictions, and observations. J Geophys Res 91:9407–9446
Hon K, Kauahikaua JP, Denlinger R, Mackay K (1994) Emplacement and inflation of pahoehoe sheet flows: observations and measurements of active lava flows on Kilauea, Hawai'i. Geol Soc Am Bull 106:351–370
Hulme G (1974) The interpretation of lava flow morphology. Geophys J R Astr Soc 39:361–383
Ishihara K, Iguchi M, Kamo K (1990) Numerical simulation of lava flows on some volcanoes in Japan. In: Fink JH (ed) Lava flows and domes. Springer, Berlin Heidelberg New York, pp 184–207
Kays WM, Crawford ME (1980) Convective heat and mass transfer. McGraw-Hill, New York, pp 1–420
Keszthelyi L (1994) Calculated effect of vesicles on the thermal properties of cooling basaltic lava flows. J Volcanol Geotherm Res 63:257–266
Keszthelyi L (1995a) A preliminary thermal budget for lava tubes on the Earth and planets. J Geophys Res 100:20411–20420
Keszthelyi L (1995b) Measurements of the cooling at the base of pahoehoe flows. Geophys Res Lett 22:2195–2198
Keszthelyi L, Denlinger R (1996) The initial cooling of pahoehoe flow lobes. Bull Volcanol 58:5–28
Keszthelyi L, Self S (1998) Some physical requirements for the emplacement of long basaltic lava flows. J Geophys Res 103:27447–27464
Keszthelyi L, McEwan AS, Thordarson T (2000) Terrestrial analogs and thermal models for Martian flood lavas. J Geophys Res 105:15027–15049
Klingelhöfer F, Hort M, Kümpel H-J, Schmincke H-U (1999) Constraints on the formation of submarine lava flows from numerical model calculations. J Volcanol Geotherm Res 92:215–229
Lipman PW, Banks NG (1987) Aa flow dynamics, Mauna Loa 1984. US Geol Surv Prof Pap 1350:1527–1567
Lockwood JP, Banks NG, English TT, Greenland LP, Jackson DB, Johnson DJ, Koyanagi RY, McGee KA, Okamura AT, Rhodes JM (1985) The 1984 eruption of Mauna Loa volcano, Hawaii. EOS Trans Am Geophys Union 66:169–171
Lockwood JP, Dvorak JJ, English TT, Koyanagi RY, Okamura AT, Summers ML, Tanigawa WR (1987) Mauna Loa 1974–1984: a decade of intrusive and extrusive activity. US Geol Surv Prof Pap 1350:537–570
Mangan M, Castro J, Cashman KV, Loewenberg M (1998) Rheology of bubble-bearing magmas. J Volcanol Geotherm Res 87:15–28
McBirney AR, Noyes RM (1979) Crystallization and layering of the Skaergaard intrusion. J Petrol 20:487–554
Moore HJ (1987) Preliminary estimates of the rheological properties of 1984 Mauna Loa lava. US Geol Surv Prof Pap 1350:1569–1588
Murase T, McBirney AR (1973) Properties of some common igneous rocks and their melts at high temperatures. Geol Soc Am Bull 84:3563–3592
Oppenheimer C (1991) Lava flow cooling estimated from Landsat Thematic Mapper Infrared data: the Lonquimay eruption (Chile, 1989). J Geophys Res 96:21865–21878
Peck DL (1978) Cooling and vesiculation of Alae lava lake, Hawaii. US Geol Surv Prof Pap 935-B:1–59
Pinkerton H, Sparks RSJ (1976) The 1975 sub-terminal lavas, Mount Etna: a case history of the formation of a compound lava field. J Volcanol Geotherm Res 1:167–183
Pinkerton H, Sparks RSJ (1978) Field measurements of the rheology of lava. Nature 276:383–385
Pinkerton H, Stevenson RJ (1992) Methods of determining the rheological properties of magmas at sub-liquidus temperatures. J Volcanol Geotherm Res 53:47–66
Pinkerton H, Wilson L (1994) Factors controlling the lengths of channel-fed lava flows. Bull Volcanol 56:108–120
Robertson EC, Peck DL (1974) Thermal conductivity of vesicular basalt from Hawaii. J Geophys Res 79:4875–4888
Rowland SK, Walker GPL (1990) Pahoehoe and aa in Hawaii: volumetric flow rate controls the lava structure. Bull Volcanol 52:615–628
Ryan MP Sammis CG (1981) The glass transition in basalt. J Geophys Res 86:9519–9535
Shaw HR, Peck DL, Okamura R (1968) The viscosity of basaltic magma: an analysis of field measurements in Makaopuhi lava lake, Hawaii. Am J Sci 263:120–152
Sparks RSJ, Pinkerton H (1978) Effect of degassing on rheology of basaltic lava. Nature 276:385–386
Sparks RSJ, Pinkerton H, Hulme G (1976) Classification and formation of lava levees on Mount Etna, Sicily. Geology 4:269–271
Tallarico A, Dragoni M (1999) Viscous newtonian laminar flow in a rectangular channel: application to Etna lava flows. Bull Volcanol 61:40–47
Tanguy J-C (1973) The 1971 Etna eruption: petrology of the lavas. Phil Trans R Soc Lond 274:45–53
Tanguy J-C, Clocchiatti R (1984) The Etnean lavas, 1977–1983: petrology and mineralogy. Bull Volcanol 47:879–894
Tonarini S, Armienti P, D'Orazio M, Innocenti F, Pompilio M, Petrini R (1995) Geochemical and isotopic monitoring of Mt. Etna 1989–1993 eruptive activity: bearing on the shallow feeding system. J Volcanol Geotherm Res 64:95–115
Wilmoth RA, Walker GPL (1993) P-type and S-type pahoehoe: a study of vesicle distribution patterns in Hawaiian lava flows. J Volcanol Geotherm Res 55:129–142
Wilson M (1989) Igneous petrogenesis. Allen and Unwin, Australia, pp 1–466
Wolfe ES, Morris J (1996) Geologic map of the Island of Hawaii. US Geol Surv Misc Invest Ser Map I-2524-A
Wolfe EW, Neal CA, Banks NG, Duggan TJ (1988) Geologic observations and chronology of eruptive events. US Geol Surv Prof Pap 1463:1–97
Wooster MJ, Wright R, Blake S, Rothery DA (1997) Cooling mechanisms and an approximate thermal budget for the 1991–1993 Mount Etna lava flow. Geophys Res Lett 24:3277–3280
Wright TL, Okamuara RT (1977) Cooling and crystallization of Tholeiitic Basalt, 1965 Makaopuhi lava lake, Hawaii. US Geol Surv Prof Pap 1004:1–78